Miocene tectono-sedimentary evolution of the eastern external Betic Cordillera (Spain)

Manuel Martín-Martín, Francesco Guerrera, Tomás Rodríguez-Estrella, Francisco Serrano, Francisco J. Alcalá, Giuliana Raffaelli & Mario Tramontana

Published online: 13 Jul 2018.

Submit your article to this journal

Article views: 60

View Crossmark data

Taylor & Francis
Taylor & Francis Group

ARTICLE

Miocene tectono-sedimentary evolution of the eastern external Betic Cordillera (Spain)

Manuel Martín-Martín [a], Francesco Guerrera[b], Tomás Rodríguez-Estrella[c], Francisco Serrano [d], Francisco J. Alcalá [e,f], Giuliana Raffaelli[b] and Mario Tramontana [g]

aDepartamento de Ciencias de la Tierra y Medio Ambiente, Universidad de Alicante, Alicante, Spain; bEx-Dipartimento di Scienze della Terra, della Vita e dell'Ambiente, Università degli Studi di Urbino Carlo Bo, Italy; cDepartamento de Ingeniería Minera, Geológica y Cartográfica, Universidad Politécnica de Cartagena, Spain; dDepartamento de Ecología y Geología, Universidad de Málaga, Spain; eDepartamento de Ingeniería Civil, Universidad Católica de Murcia, Spain; fInstituto de Ciencias Químicas Aplicadas, Universidad Autónoma de Chile, Chile; gDipartimento di Scienze Pure e Applicate, Università degli Studi di Urbino Carlo Bo, Italy

ABSTRACT

An interdisciplinary study of Miocene successions in the eastern External Betic Zone (South Iberian Margin) was carried out. Evidences of syn-sedimentary tectonic activity were recognized. The results enabled a better reconstruction of the stratigraphic architecture (with an improved chronostratigraphic resolution) in the framework of the Miocene foredeep evolution of the eastern EBZ. Two main depositional sequences were dated as uppermost Burdigalian-upper Serravallian *p.p.* and middle-upper Tortonian. *p.p.*, respectively. The vertical and lateral diversification of lithofacies associations and thicknesses resulted from the syn-depositional tectonic complexity of the area. A great variety of sedimentary depositional realms is due to different subsidence rates, and the growing of anticlines and synclines during the Langhian *p.p.*-Serravallian. After a regression with an early Tortonian erosional gap, platform to hemipelagic realms developed during the middle Tortonian. The end of the sedimentation coincided with the emplacement of an important olisthostrome-like mass consisting of Triassic material related to either the development of thrust systems or diapirs emerged in the middle-late Tortonian, during the nappe emplacement. Correlations with other external sectors of the Betic Chain, and the external domains of the Rif, Tell, and northern Apennine Chains highlighted a similar Miocene foredeep evolution during the building of these orogens.

1. Introduction

The study area belongs to the eastern External Zone of the Betic Cordillera (Spain, Figure 1(A)). This cordillera and the Rif Chain (Morocco) constitute the Betic-Rifian Arc that represents the westernmost Mediterranean Alpine orogenic belt originated by a Miocene tectonics.

The External Betic Zone (EBZ) consists of the Mesozoic to Tertiary sedimentary cover of the South Iberian Margin (Figure 1(B)). This passive Alpine margin started to develop during the Mesozoic rifting of the western Tethys that caused the formation of deep and shallow marine pelagic successions separated by normal faults. In the region a Cretaceous tectonic inversion from extension to compression occurred, similarly to what was observed in the western Mediterranean Alpine chains (Guerrera et al., 2014; Guerrera & Martín-Martín, 2014a; *and references therein*). In the EBZ the Mesozoic normal faults evolved during the Tertiary under compressive deformation as strike-slip faults, and later as thrusts (Sanz de Galdeano & Buforn, 2005; Martín-Martín et al.,

2018a; Martín-Martín, Guerrera, Alcalá, Serrano, & Tramontana, 2018b; Sissingh, 2008). In the Miocene many intramontane basins developed whose geometry and stratigraphic architecture were controlled by re-arrangements of blocks and faults. These intramontane basins were related to the evolution of the North Betic Strait (or Proto-Guadalquivir Foreland Basin) that represented a foredeep area connecting the Atlantic Ocean and the Mediterranean Sea during a part of the Miocene (Sanz De Galdeano & Vera, 1992).

Most of knowledges about the Tertiary sediments of these intramontane basins in the eastern EBZ appear in old papers. Recent studies are mainly focused on Paleogene evolution (e.g. Guerrera et al., 2006, 2014; Guerrera & Martín-Martín, 2014a) and late Miocene bio-chronostratigraphy (e.g. Garcés, Krijgsman, & Agustí, 2001; Lancis et al., 2010). This paper tries to fill the current gap concerning the Miocene stratigraphic evolution of the eastern EBZ through an interdisciplinary study taking advantage both from the good quality of outcrops and the continuity of the stratigraphic record in the Sierra del Carche-Pinoso Corridor-Sierra de la Pila sector. The
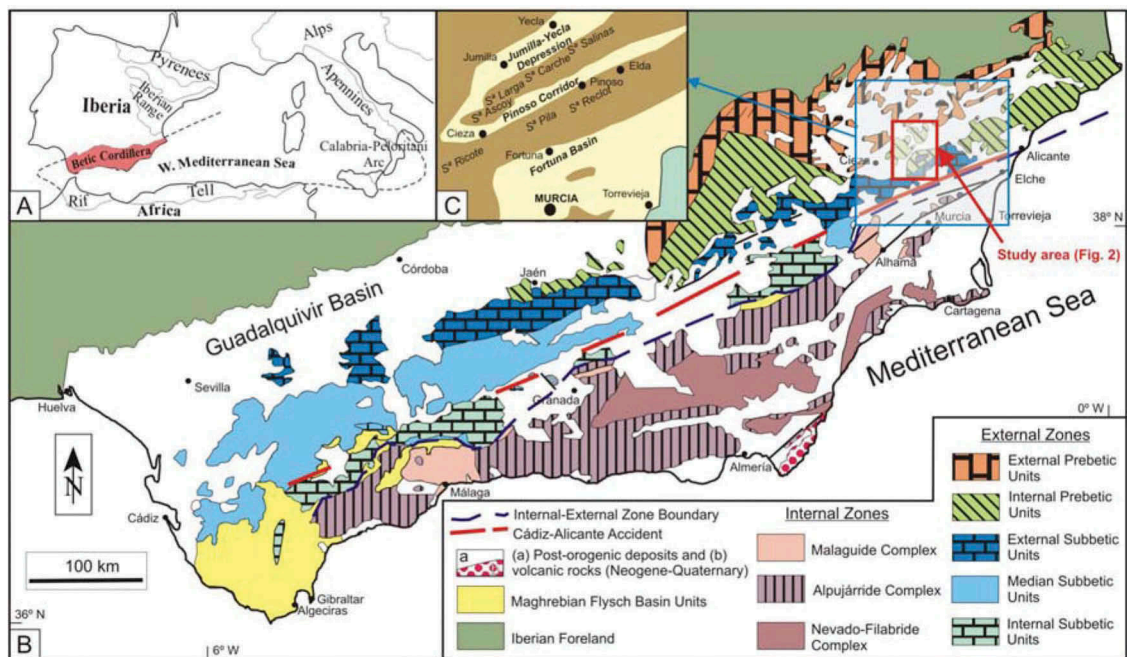
Figure 1. (A) Location of the Betic Cordillera in the central-western Mediterranean area. (B) Geological map of the Betic Cordillera (simplified and modified after Vera, 2000, 2004) with the location of the study area. (C) Geographical sketch showing localities and geological features mentioned in the text.

results were compared and completed with the previous studies concerning the EBZ (Sanz De Galdeano & Buforn, 2005; Guerrera et al., 2014; Martín-Martín et al., 2018a, 2018b; and references therein).

Data were used to reconstruct the Miocene stratigraphic evolution of the eastern EBZ based on methodological criteria established in the previous interdisciplinary studies both in the Betic Chain (e.g. Guerrera et al., 2014; Guerrera & Martín-Martín, 2014a) and otherchains (e.g. Belayouni et al., 2009, 2006; Belayouni, Guerrera, Martín-Martín, & Serrano, 2013). The logic was to make comparison between the External Betic sector and other external domains of the northern Africa (Rif and Tunisian Tell) and Apennine Chain in order to highlight common regional tectonic events for a better comprehension of the Miocene evolution of the central-western Mediterranean region.

2. Geological setting

The Betic Cordillera is traditionally subdivided into the Internal Betic Zone (IBZ), External Betic Zone (EBZ) and 'Campo de Gibraltar Complex', the latter belonging to the Maghrebian Flysch Basin (MFB) Zone (Figure 1). Similar to other sectors of the Maghrebian Chain (Rif, Algeria-Tunisia Tell, Sicily, and southern Apennines), and the northern Apennines, the structure of the Betic Cordillera shows the IBZ overriding the MFB units, which are therefore sandwiched between the former and the EBZ (De Capoa, Di Staso, Guerrera, Perrone, & Tramontana, 2003; Bonardi et al., 2003; Perrone, Di Staso, & Perrotta, 2008; Perrone, Perrotta, Marsaglia, Di Staso, & Tiberi,

2014; Di Staso, Perrotta, Guerrera, Perrone, & Tramontana, 2009; Guerrera & Martín-Martín, 2014a; and references therein).

The Tertiary Africa-Iberia convergence (and related subduction) and the opening of the Alboran area as a back-arc basin caused folding, thrusting, and strike-slip faulting that controlled the paleogeography and the evolution of the basin-margin systems. During the Cretaceous-Paleogene a gentle basement flexure also affected the overlying successive sedimentation, resulting in some lateral lithofacies changes and unconformities (e.g. Guerrera et al., 2006, 2014; Guerrera & Martín-Martín, 2014b). During the early Miocene the region underwent to an E-W compression that rotated at about N-S from the middle Miocene (De Ruig, 1992; Sanz De Galdeano & Buforn, 2005). The Miocene nappe stacking started in the innermost EBZ while a major strike-slip faulting occurred in a large portion of the outermost EBZ (Sanz De Galdeano & Vera, 1992). Because of this deformation the main faults acted as strike-slip faults during most of the Miocene, bringing about corridor-shaped intramontane basins and mountain alignments bounded by N70°E, N155°E, and N120°E trending fault systems as in the study area.

The EBZ consist of SW-NE aligned ridges related to similarly trending folds and thrusts separating narrow depressions (corridors) filled with Miocene-Quaternary sediments (Figure 1(C)). The EBZ is usually subdivided into two main sub-domains: (1) the Prebetic which represents a platform realm stratigraphically continuous with the foreland (Iberian Meseta); and (2) the unrooted Subbetic (located south of the previous

one) which represents a deeper area corresponding to the Internal, Median, and External Subbetic sub-zones. Both sub-domains are characterized by Triassic to Tertiary sedimentary successions progressively deformed from south to north during the middle-late Miocene to generate a pile of nappes (Vera, 2000; Arias et al., 2004; *and references therein*). The presence of major unconformities led Vera (2004) to define VIII Main Sedimentary Cycles for the EBZ (Figure 2).

The study area corresponds to the Sierra de El Carche (SC), Pinoso Corridor (PC), and Sierra de La Pila (SP) sectors (Figure 2(A)), where several structural sub-zones can be distinguished as a result of different fault systems (Figure 2): E-W, NW-SE, and N-S dextral strike-slip faults; SW-NE sinistral strike-slip faults; and W-E to SW-NE, N-S, and NW-SE normal faults.

3. Methods

The Miocene stratigraphic record of the Sierra de El Carche (SC) (Logs 5 and 6 *p.p.*), Pinoso Corridor (PC) (Log 6 *p.p.*), and Sierra de La Pila (SP) (Logs 1 to 4) sectors (Figure 2) was reconstructed by means of six representative stratigraphic sections. In Logs 1 to 6, 95 samples (Figure 3) were collected for different analyses (biostratigraphy, mineralogy, and petrography). Based on the main Sedimentary Cycles of Vera (2000, 2004) a specific geological map (Figure 2) including a tectonic sketch of the main structures and location of stratigraphic sections was realized.

For the chronologic control of deposition, biostratigraphic studies on planktonic foraminifera of 80 samples (Figures 3) were performed. The bio-chronostratigraphic scheme was based on the standard zonal scale by Blow (1969), the Global Standard Chronostratigraphic Scale (Lourens, Hilgen, Laskar, Shackleton, & Wilson, 2004; Hilgen et al., 2005, 2009; *and references therein*), and the most significant foraminiferal bio-events in the Mediterranean during the Miocene.

A Phillips X'PERT MPD Systempert ® diffractometer with an automatic slit, CuKα radiation, and 2 to 6°min⁻¹ scanning interval from 2° 2θ to 60° 2θ was used to examine the whole-rock and the < 2 μm grain-size fraction (clay fraction) mineralogy of 44 samples (Figure 3) from the SC (10 samples; Logs 5, 6 *p.p.*), PC (8 samples; Log 6 *p.p.*), and SP (26 samples; Logs 1, 2) successions. The crystalline-powder technique was used for mineral identification in the whole-rock. For the non-calcareous clay fraction, oriented mounts on glass slides were prepared and analyzed as described in Alcalá, López-Galindo, and Martín-Martín (2013a) and Martín-Martín et al. (2018b).

A Nikon TK-1270E ® polarized-light optical microscope equipped with a digital camera for image acquisition was used to study the arenite petrography of 15 samples (11 from SC and 4 from SP).

4. Results

4.1. *Lithostratigraphy*

Three main formations were recognized in all studied sectors: the Congost, Lower Tap, and Upper Tap Formations. The Congost Formation was previously defined by Tent-Manclús (2003), meanwhile a Tap Formation was defined by Vera (2000). The Congost Formation (Figure 3) unconformably overlies the Miñano and Murtas Formations (Guerrera & Martín-Martín, 2014a) consisting of Eocene Nummulite limestones, and Oligocene-Aquitanian lacustrine limestones and fluvial conglomerates, respectively. The Congost Formation was subdivided into four lithofacies (C to F) and progressively passes laterally and upwards to the Lower Tap Formation. In this paper, the previously defined Tap Formation has been divided into the Lower and Upper Tap Formations separated by a recognized unconformity with a related gap of about 3 Ma. The Lower Tap Formation was subdivided into 5 lithofacies (G to N) and shows more lateral and upward lithofacies variations compared to the Congost Formation. The Upper Tap Formation was subdivided into four lithofacies (O to R). In the study area, the Upper Tap Fm is unconformably covered by Pliocene to Quaternary deposits (Lithofacies S). Stratigraphic data, tectonic contacts, unconformities, samples, thicknesses, and lithofacies defined in the studied successions are listed in Table 1 and represented in Figure 3.

4.2. *Sedimentology*

Sedimentological features of the above mentioned formations have been studied with the aim to define the sedimentary realm of different recognized lithofacies and in particular taking into account lithotypes, sedimentary structures, carbonate and arenite microfacies and fossil content. Special attention has been addressed to relationships between planktonic and benthonic foraminifera assemblages. The main sedimentological results are shown in Table 2 and some pictures of field details are exposed in Figure 4.

Congost Formation. This unit displays a great variety of shallow marine realms: (i) lagoon and shore marked by calcarenites with a foreshore parallel and wavy lamination (Figure 4(A)), bioturbation, and mollusk fragments (Lithofacies C), ostracods and echinoderm clasts with dominance of very significant benthic foraminifera (*Ammonia*); (ii) internal and external platform to biostrome front, characterized by biocalcarenites (Lithofacies D) containing preserved bivalves (frequent ostreids) (Figure. 4(B)) and predominance of planktonic foraminifera; (iii) internal to external platform with massive algal biocalcarenites and marls (Lithofacies E) with red algae (Figure. 4(C)); (iv) external platform to upper slope (Lithofacies F) with marls and stratified biocalcarenites (Figure. 4(D)), nodular and reefal
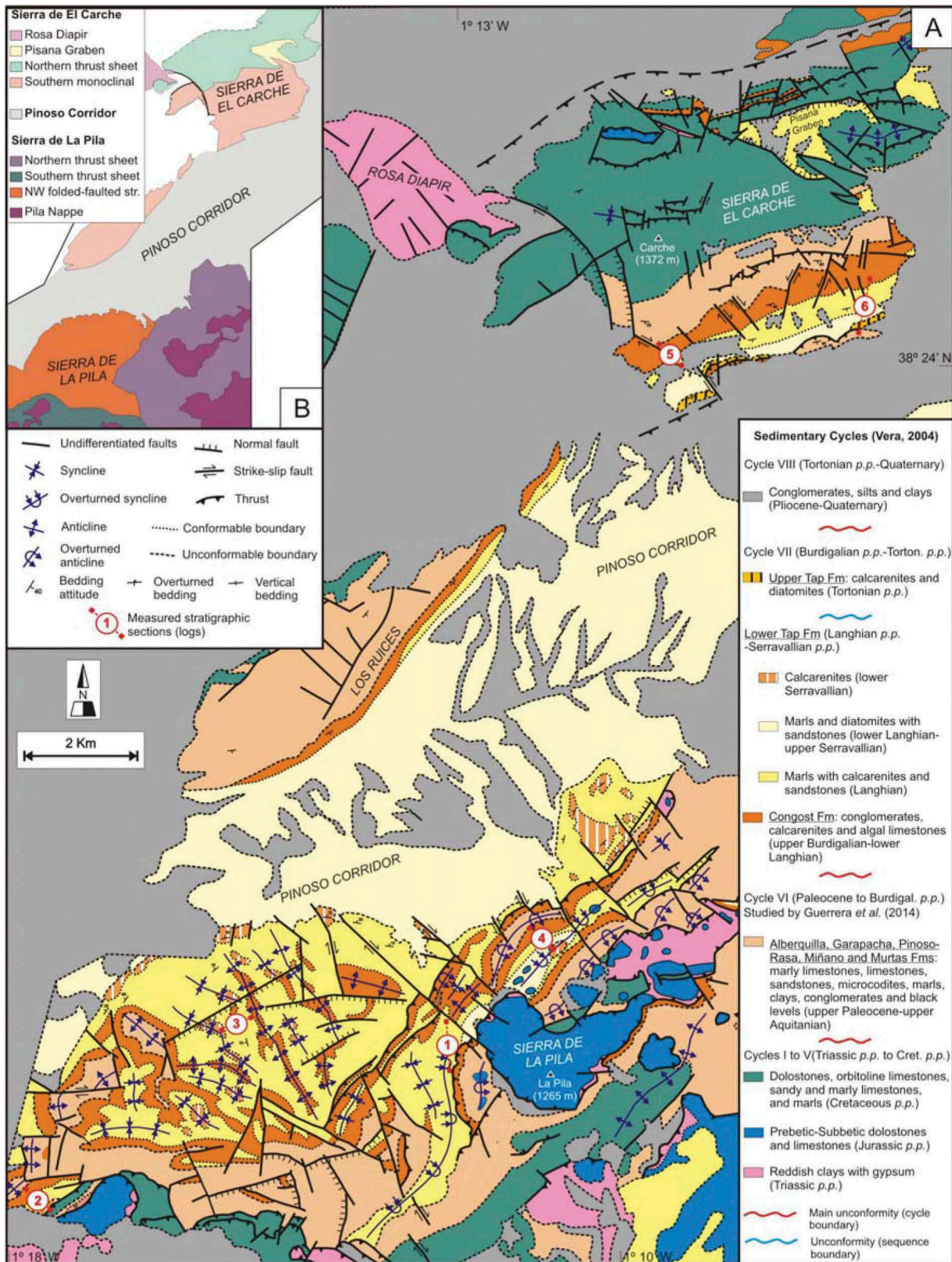
Figure 2. (A) Detailed geological map based on the Main Sedimentary Cycles of Vera (2000, 2004) showing the three study sectors: Sierra de El Carche, Pinoso Corridor, and Sierra de La Pila; location of the measured logs as in Figure 3 is also indicated. (B) Structural sketch map showing the different structural zones and sub-zones described in the text.

structures, biostromes and preserved bivalves, dominance of planktonic foraminifera, and presence of sponge spicules and echinoderms.

Lower Tap Formation. This formation displays several marine realms that are deeper than those of the

Congost Formation: (i) external platform to upper slope (Lithofacies G) with sandy marls and biocalcarenite intercalations showing marked prevalence of planktonic foraminifera and presence of sponge spicules and echinoderms; (ii) slope (Lithofaies H)
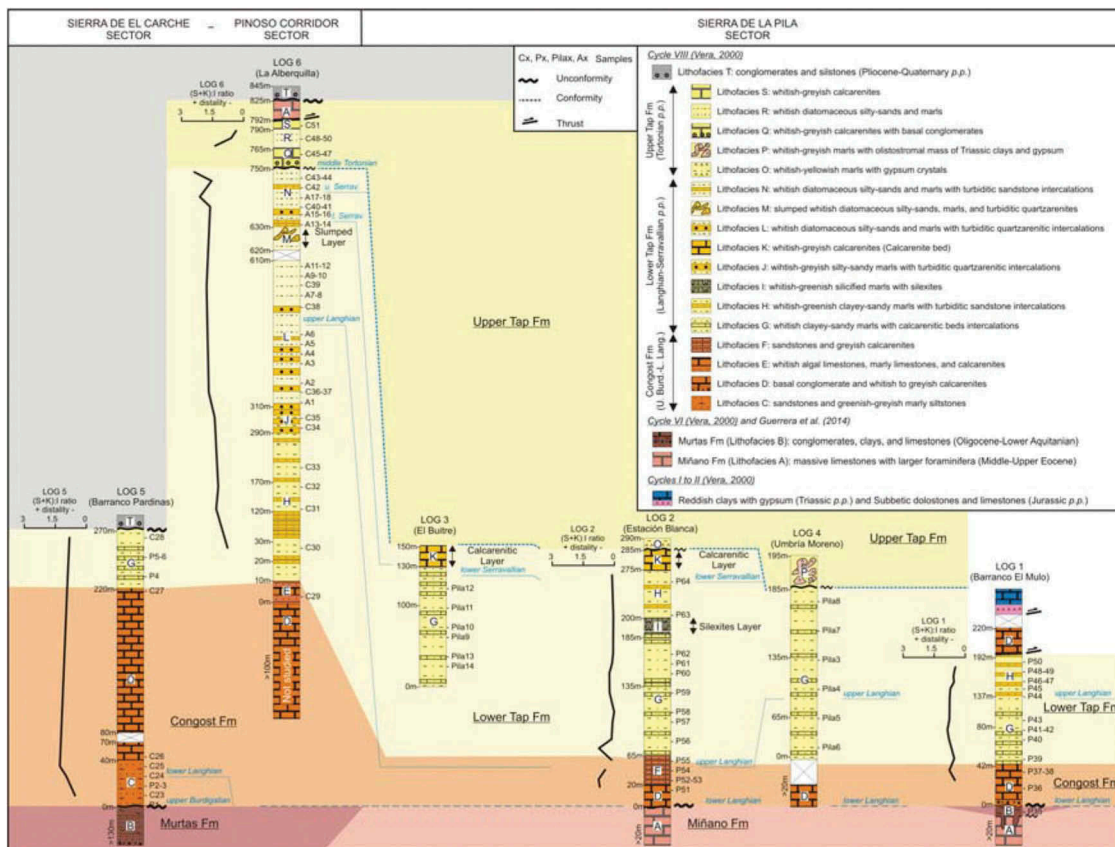
Figure 3. Lithostratigraphic record, lateral correlations, and unconformities recognized in the six representative successions reconstructed in the study area (location in Figure 2); details about lithofacies and boundaries in Table 1. Correlation of the local relative sea-level curve deduced from the dimensionless (S + K):I ratio in the studied Sierra de El Carche (left), Pinoso Corridor (center), and Sierra de La Pila (right) successions is also reported; see the original values in Table 4.

characterized by marls and turbiditic sublitharenites with Bouma intervals (Figure. 4(F,G)) and a marked prevalence of planktonic foraminifera, with also sponge spicules and echinoderms; (iii) deep basin with silexitic marls (Lithofacies I) containing radiolarians (Figure 4(H)); (iv) slope (Lithofacies J and L) with lenticular quartzarenite turbidites with Bouma intervals and diatomaceous marls, and with predominance of planktonic foraminifera; (v) internal platform with algal biocalcarenites and marly intercalations (Lithofacies K); (vi) slope with diatomaceous silty sands (Litofacies M) and deformed (slump) turbiditic arenites (Figure 4(I)); (vii) external platform to upper slope with diatomaceous silty sands (Litofacies N) and deformed (slump) turbiditic quartzarenites, and dominance of benthic foraminifera, and with sponge spicules and echinoderms.

Upper Tap Formation. This unit displays several deep to shallow marine realms: (i) slope with olisthostrome deposits (Lithofacies O and P) consisting of reworked Triassic material (Figure 4(J)); (ii) internal platform with biostromic calcarenite bodies (Lithofacies Q) with cross bedding (Figure 4(K)) and bivalves (frequent ostreids); (iii) external platform with diatomaceous silty sands (Litofacies R) made up of mudstones with diatomites (Figure 4(L)), with high

prevalence of benthic foraminifera, and sponge spicules; (iv) internal platform with biostromic calcarenite bodies (Lithofacies S).

4.3. *Biostratigraphy and chronostratigraphy*

Congost Formation. It could begin towards the Burdigalian-Langhian passage (Figure 5) by considering that the *G. trilobus* group including *G. bisphaericus* (see Table 3 for formal names) appears from the lowest levels of the formation, and the presence of *P. sicanus* is uncertain due to poor preservation. The upper part (lithofacies D) provides assemblages made up predominantly by *Globoquadrina* and the plexus *Globigerinoides* gr. *trilobus-Praeorbulina* with *P. sicanus* and *P. glomerosa*, which are characteristic of the upper N8 zone of the lower Langhian. The top of the formation (lithofacies F; Log 2, P53-P55) contains *O. suturalis*, marking the N9 Zone and thus belonging to the upper Langhian.

Lower Tap Formation. Based on the presence of *Praeorbulina*, the lithofacies (G) of this formation is lower Langhian in the SP sector (Log 1, P39; Log 4, Pila6). The occurrence of *Orbulina* in successive levels (P44 and Pila7) already denotes deposition of the upper Langhian. Lithofacies I (Log 2) can be attributed

Table 1. Main lithostratigraphic field data (logs, localities, coordinates, thicknesses, samples, lithofacies, and boundary types) from the lithostratigraphic successions of the Sierra de El Carche (SC), Pinoso Corridor (PC), and Sierra de La Pila (SP) sectors.

Log Locality Sector	Location	Lithofacies	Thickness (m)	Samples	Description of Lithofacies, clasts sources, and geological boundaries features
1 Barranco de El Mulo (SP)	38°15′ 05″ N,1°12′ 18″ W, 692 m – 38°16′ 16″ N,1°12′ 52″ W, 779 m	A	> 30		grayish recrystallized micritic limestones with Nummulites
					Tectonic contact (thrust)
		H	55	P45÷ P50	whitish sandy clayey marls with intercalations of turbiditic arenites (N190-200°-oriented flute casts)
		G	95	P39÷ P44	whitish sandy clayey marls with well-stratified grayish calcarenites intercalated
		D	42	P36÷ P38	1 m thick basal conglomerate (transgression) with poor-rounded carbonatic clasts followed by 3–10 cm thick well-stratified grayish calcarenites affected by intense cleavage
					Angular unconformity
		B	2		reddish, greenish-gray, and whitish clays (probable continental-lagoon transition)
					Unconformity (paleokarst erosive surface with dikes)
		A	> 50	P35	20–50 cm thick stratified grayish recrystallized micritic limestones with Nummulites; karst structures filled by reddish continental clays in the upper 20 m
2 Estación Blanca (SP)	38°14′ 22″ N,1°18′ 47″ W, 320 m – 38°14′ 18″ N,1°18′ 37″ W, 308 m	O	5		whitish to yellowish marls with gypsum crystals
		K	10		whitish to grayish calcarenites with marly intercalations
		H	75	P63÷ P64	whitish sandy clayey marls with intercalations of turbiditic arenites
		I	15		whitish to greenish silicified marls with silexites
		G	120	P56÷ P62	whitish sandy clayey marls with well stratified grayish calcarenites intercalated
		F	45	P52÷ P55	well stratified grayish marly limestones, 0.3–0.6 m thick algal (rhodolites) limestones, 0.5–3 m thick calcarenites, and some intervals of whitish, yellowish marls
		D	20	P51	grayish detrital laminated limestones with some marly interlaying, affected by cleavage
					Probable angular unconformity (transgression?)
3 El Buitre (SP)	38°16′ 23″ N,1°16′ 03″ W, 700 m	A	> 20		massive micritic limestones with Nummulites
		K	20		whitish to grayish massive calcarenites and algal limestones with marly intercalations at the base
		G	130	Pila9÷ Pila14	whitish to yellowish sandy marls with calcarenite intercalations
4 Umbría Moreno (SP)	38°17′ 19″ N,1°11′ 16″ W, 721 m	P	10		whitish to grayish clayey marls with reworked Triassic clays and gypsum
					Angular unconformity
		G	185	Pila3÷ Pila8	whitish to yellowish sandy marls with calcarenite intercalations
		D	> 10		not exposed
5 Barranco Pardinas (SC)	38°24′ 11″ N,1°09′ 49″ W, 688 m	T	> 5		conglomerates, sands, and pelites
		G	50	P4÷ P6; C27÷ C28	whitish sandy clayey marls with intercalations of well-stratified grayish detritic limestones
		D	140		5–20 cm thick massive grayish detritic limestones
			10		not exposed
		D	30	C26	5–20 cm thick massive grayish detritic limestones
		C	40	P1÷ P3; C23÷ C25	yellowish-greenish sands and silty-sandy marls
					Angular unconformity
		B	> 130		0.5–0.6 cm thick conglomerates with rounded carbonatic clasts with Alveolines and Nummulites, sub-rounded quartz clasts and reddish clays, and scattered carbonatic clasts interpreted as fluvial to fan-delta deposits

(Continued)

Table 1. (Continued).

Log Locality Sector	Location	Description of Lithofacies, clasts sources, and geological boundaries features	Lithofacies	Thickness (m)	Samples
6	38°25 04 ′N,1°06 54 ′W, 766 m –	conglomerates, sands, and pelites	T	> 18	
		Angular unconformity			
La Alberquilla (SC – PC)	38°24 25 ′N,1°06 59 ′W, 719 m	grayish recrystallized micritic limestones with Nummulites	A	> 30	
		Tectonic contact (thrust)			
		lens-shaped whitish-grayish biostromal calcarenites	S	2	C51
		whitish diatomaceous silty sands and marls	R	25	C48÷C50
		progradational lenticular conglomerates followed by lens-shaped whitish-grayish biostromal calcarenites	Q	15	C45÷C47
		Angular unconformity			
		whitish arenites, poor-stratified diatomaceous, and cemented silty sands with intercalations of quartzarenites and grayish arenites	N	120	C40÷C44; A13÷A18
		slump interval containing whitish diatomaceous, silty-sands and marls with turbiditic arenites	M	10	
		not exposed		10	
		whitish diatomaceous, silty sands and marls with litharenitic and quartzose turbiditic intercalations	L	300	C36÷C39; A1÷A12
		lenticular quartzarenites (sharp-edged quartz grains), and marly sands with arenitic intercalations of turbiditic arenites	J	20	C34÷C35
		marly sands with arenitic intercalations of turbiditic arenites	H	280	C30÷C33
		massive grayish arenites and calcarenites	E	10	C29
		massive grayish detritic limestones	D	> 100	

to the uppermost Langhian, since the basal level (P63) of the overlying Lithofacies H contains *G. peripheroacuta* (base of the N10 Zone). The couple *G. praemenardii*–*G. peripheroacuta*, which is considered as a reference of the lowermost Serravallian, appears near the top of the Lithofacies H (Log 2, P64). The uppermost Lithofacies K would belong to the lower Serravallian. In the SC sector, this formation begins in the lower Langhian with *Praeorbulina* in Log 6. The successive biostratigraphic references (continuation of Log 6 in the PC): Acme intervals of *P. siakensis* (Di Stefano et al., 2008) between the samples C31 and A6, the *Orbulina* datum (A7), and the first observance (FO) of *O. universa* allow the tracking of the Langhian sedimentation. Deposits close to the Langhian-Serravallian passage occur between the samples A9 and A11, as deduced from transitional morphologies between *G. peripheroronda* and *G. peripheroacuta*, and typical *G. praemenardii*. Components of the *Foshella* group (e.g. *G. peripheroronda* and *G. peripheroacuta*) persist until the level A15, thus indicating lowest Serravallian. The most noticeable in the top of the formation (Lithofacies N; A17-A18 and C43) is the appearance of *G. menardii* and the absence of components more recent than the upper Serravallian.

Upper Tap Formation. In the PC sector, above the unconformity the Lithofacies R yielded Tortonian assemblages. The lowest level (C48) contains *N. acostaensis* (with right-and left-coiled specimens), *G. menardii*, and *G. obliquus*, an assemblage characterizing the N16 Zone (middle part of the Tortonian). Upper levels (C49) show *G. plesiotumida, G. extremus*, and *N. acostaensis-humerosa* plexus predominantly right-coiled. Thus, considering that the FO of *G. plesiotumida* marks the beginning of the N17 Zone and using the dex/sin coiling shift of the *Neogloboquadrina* populations as a reference for the middle/upper Tortonian boundary (Serrano, Palmqvist, Guerra-Merchán, & Romero, 1995), these beds must have been deposited close to the end of the middle Tortonian. In fact, in the following level (C50) *Neogloboquadrina* shows a predominant left coiling, suggesting deposition already of the upper Tortonian. In the SP sector, a marked cartographic unconformity is well recognized in Logs 2 and 4 separating the Lower and Upper Taps Formations. Nevertheless, Lithofacies O (Log 2) and Lithofacies P (Log 4) from the Upper Tap Formation have not yielded fossils of biostratigraphic relevance.

4.4. Mineralogy and petrography

The whole-rock mineralogy in the SC (Logs 5, 6 *p.p.*), PC (Log 6 *p.p.*), and SP (Logs 1, 2) successions includes, respectively quartz (< 5–9% and < 5–20%), calcite (20–58% and 33–84%), phyllosilicates (18–32% and < 5–31%), dolomite (5–30% and 6–35%), and minor amounts of K-feldspar, plagioclase, and gypsum
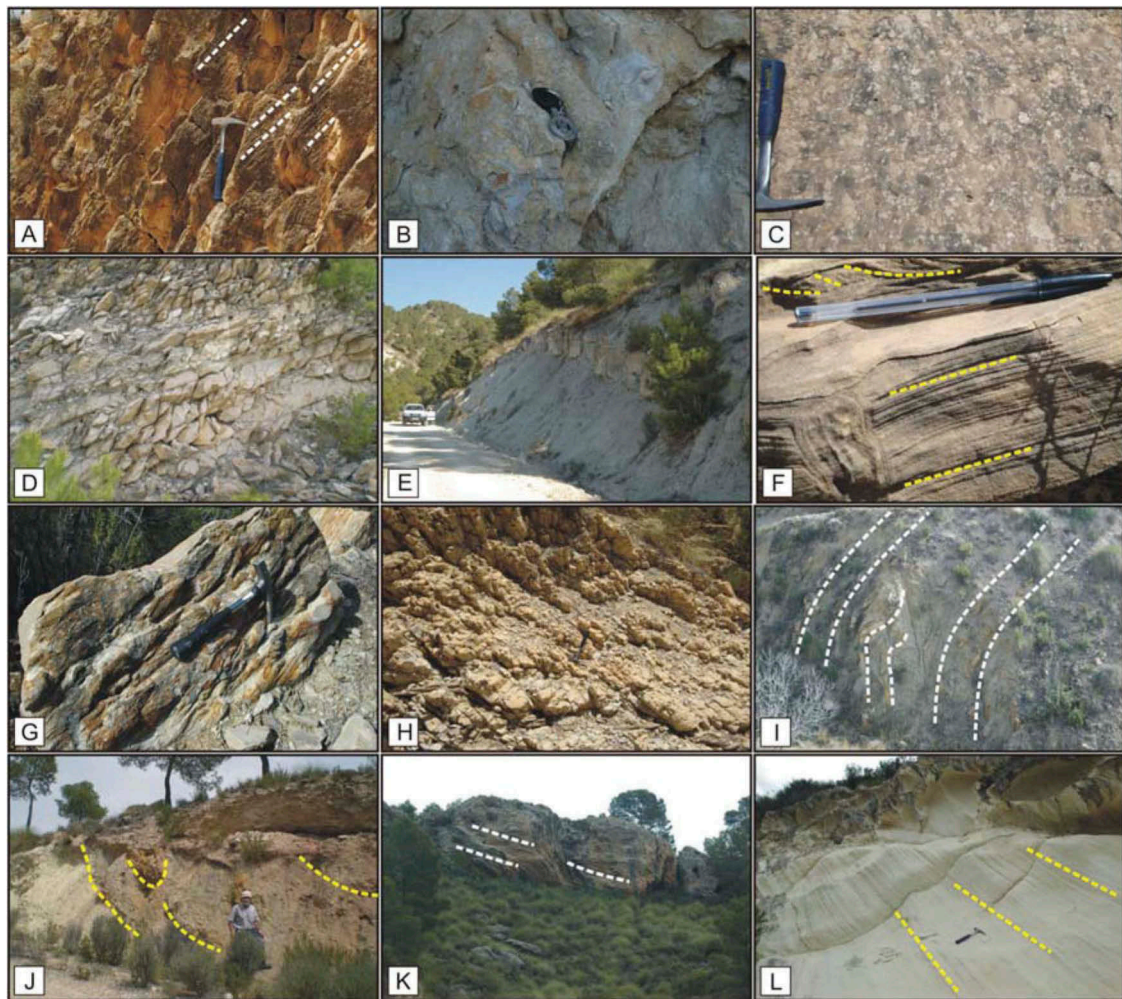
Figure 4. Photos of the Congost (A TO D), Lower Tap (E to I), and Upper Tap (J to L) Formations showing sedimentological details. (A) laminated foreshore sandstones (Lithofacies C); (B) calcarenites with ostreids (Lithofacies D); (C) algal limestones (Lithofacies E); (D) calcarenites with close spaced jointing (Lithofacies F); (E) marls with calcarenite intercalations (Lithofacies G); (F) turbidite sandstone with Ta-c Bouma intervals (Lithofacies H); (G) flute casts at the base of a turbidite sandstone bed (Lithofacies H); (H) silexites with close spaced jointing (Lithofacies I); I) slump consisting of marls and turbidite sandstones (Lithofacies M); (J) marls (to the left) and an olisthostrome (to the right) containing Triassic reworked clays and gypsums (Lithofacies P) topped by Quaternary unconformable conglomerates; (K) cross-bedded calcarenites (Lithofacies Q); (l) diatomaceous marls (Lithofacies R).

in the SC and PC sectors only (Table 4). In the SC and PC successions, quartz is quite homogeneous, and the carbonate fraction (calcite and dolomite) and phyllosilicates vary somewhat more (Figure 6(A)), thus indicating relatively stable supplies of these minerals. K-feldspar, plagioclase, and gypsum are systematically found in all samples, except gypsum in some samples of Lithofacies C and D (Log 5) in the Congost Formation in the SC sector, thus suggesting a continuous minor supply of reworked Triassic materials (Martín-Martín et al., 2018b) rich in these minerals (Dorronsoro, 1978). Regarding the SC and PC successions, the SP successions show (Figure 6(C)): (1) more heterogeneous amounts of quartz, carbonate fraction, and phyllosilicates, thus suggesting a more proximal and fluctuating carbonate- vs. terrigenous-rich mineral supply with predominance of the carbonate one; (2) increasing abundance of quartz from the

Congost Formation to the Lower Tap Formation, thus indicating a more terrigenous influence in the second one; (3) higher; (4) occurrence of K-feldspar and plagioclase only in the Lithofacies G and H (Log 1), and I (Log 2); and (5) absence of gypsum both in the Congost and Lower Tap Formations.

The clay-fraction mineralogy in the SC (Logs 5, 6 *p. p.*), PC (Log 6 *p.p.*), and SP (Logs 1, 2) successions includes, respectively smectite (29–57% and 16–46%), illite (24–52% and 37–65%), random mixed-layer illite-smectite (I-S) (5–16% and < 5–25%), and kaolinite (< 5–21% and < 5–17%) (Table 4). The clay-mineral association smectite+ illite±(I-S)+ kaolinite characterizes the SC, PC, and SP successions (Figure 6 (B, D)), thus suggesting a same and main source area from Cretaceous-Paleogene terrains (Alcalá, Guerrera, Martín-Martín, Raffaelli, & Serrano, 2013b; Alcalá et al., 2013a; Alcalá, Martín-Martín, & López-Galindo, 2001)

Table 2. Main sedimentological data of the successions of Sierra de El Carche (SC), Pinoso Corridor (PC), and Sierra de La Pila (SP) sectors.

Litho-stratigraphy	Lithofacies (description in Table 1)	Age	Lithotypes	Sedimentary structures	Petrofacies	Biomicrofacies (< 150µm)	Further significant fossiliferous content	Sedimentary Realm
Upper Tap Formation	S (Log 6)	Middle Tortonian *p.p.*	Lens-shaped biostromal calcarenites	Q = Cross bedding, progradation	Litharenites, Bioclastic packstones	– –	– –	Internal platform
	R (Log 6)		Diatomaceous silty sands and marls	Thin laminae	Biomicritic limestones (Mudstone)	- Highly predominant benthic forams; - Frequent sponge spicules	Diatomites	External platform
	Q (Log 6)		Lens-shaped biostromal conglomerates and calcarenites	Q = Cross bedding, progadation; prograding lenticular conglomerates	Litharenites, Bioclastic packstones	– –	Bivalves (frequent ostreids)	Internal platform
Lower Tap Formation	N (Log 6)	Lower Serravallian *p.p.* Upper Langhian *p.p.*	Poorly stratified diatomaceous, silty sands with intercalations of quartzarenites, and arenites	Graded bedding, Bouma intervals	Biomicritic limestones (Mudstone)	- Predominant benthic forams; - Abundant sponge spicules and radiolarians	Diatomites	External platform to upper slope (fine terrigenous supply)
	M (Log 6)		Deformed diatomaceous silty-sands and marls with turbiditic arenites	Graded bedding, Slump	– –	– –	– –	Slope
	K (Logs 2, 3)		Calcarenite beds with marly intercalations	Marked bedding	Biocalcarenites	– –	Algae	Internal platform
	L (Log 6)		Diatomaceous silty sands and marls with litharenitic and quartzose turbiditic intercalations	Graded bedding, Bouma intervals channelization, groove N10°-190°	Biocalcarenites, Quartzarenites	- Highly predominant planktonic forams; - Frequent sponge spicules and radiolarians	– –	Slope with quartzarenitic supply
	J (Log 6)		Lenticular quartzarenites (sharp-edged quartz grains) alternating with marly sands and arenites	Graded bedding, Bouma intervals, channelization, groove N10°-190°	Litharenites, Quartzarenites	- Predominant planktonic forams	– –	
	I (Log 2)		Silicified marls with silexites	Marked bedding	– –	– –	Radiolaria	Slope to deep basin
	H (Logs 1, 2, 6)		Sandy clayey marls with intercalations of turbiditic arenites	Graded bedding, Bouma interval, flutes to N190°-200°	Sub-litharenites, Biocalcarenites	- Highly predominant planktonic forams; - Subordinate benthic forams, sponge spicules, and echinoderms	– –	Slope with terrigenous supply
	G (Logs 1, 2, 3, 4, 5)		Sandy clayey marls with intercalations of calcarenites	Well bedded, calcarenites/marls (c/m ratio = 30/70)	Biocalcarenites	- Predominant planktonic forams; - Subordinate benthic forams, sponge spicules, and echinoderms	– –	External platform to upper slope

(Continued)

Table 2. (Continued).

Litho-stratigraphy	Lithofacies (description in Table 1)	Age	Lithotypes	Sedimentary structures	Biomicrofacies (< 150µm)	Petrofacies	Further significant fossiliferous content	Sedimentary Realm
Congost Formation	F (Log 2)	Upper Langhian *p.p.* Lower Burdigalian *p.p.*	Marly limestones, and calcarenites	Marked bedding, lamination, nodular and reefal structures, biostromes, bivalves	- Predominant planktonic forams; - Frequent benthic forams and sponge spicules	Litharenites	Algae (Rodolites)	External platform to upper slope
	E (Log 6)		Arenites, calcarenites, and algal limestones	Massive beds	– –	Biocalcarenites	Algae	Internal/external platform
	D (Logs 1, 2, 4, 5, 6)		Calcarenites with ostreids with occasional marly interlayers	Marked bedding, laminated detritic limestones	- Predominant planktonic forams; - Frequent invertebrate clasts and benthic forams	Biocalcarenites, Siltstones	Bivalves (frequent ostreids)	Internal and External platform to biostromal front
	C (Log 5)		Sands with silty-sandy marls	lamination (foreshore), discontinuous arenite beds	Very shallow-water benthic foram (Ammonia) ostracods, and echinoderm clasts	Litharenites	Mollusk fragments	Lagoon and shore

rich in smectite, illite, and mixed layer I-S, and an additional continuous minor supply of reworked (and variably weathered) Triassic materials rich in illite and kaolinite (Dorronsoro, 1978; Martín-Martín et al., 2018b). This clay-mineral association has been described in other Proto-Mediterranean areas during the Miocene, including the external Subbetic (Alcalá et al., 2013b, 2013a; Martín-Martín et al., 2018b) and Rifian (Maaté et al., 2017) domains. In the PC successions higher and lower abundance of smectite (and associated lower and higher abundance of illite) are found in the upper part of the Lower Tap Formation (Lithofacies H to L) and in the Upper Tap Formation, respectively (Figure 6(B)). Regarding the SC and PC successions, the SP successions show: (1) lower and higher amounts of smectite and illite, which respectively decreases and increases from the Congost Formation to the Lower and Upper Tap Formations; and (2) slightly higher amounts of mixed layer I-S and kaolinite with the highest values in the Lower Tap Formation (Figure 7(D)).

The different hydrodynamic behaviour of detrital clay minerals in the marine depositional environment allows assessment of supplies distality induced by relative sea-level variations (Daoudi, Deconinck, Witan, & Rey, 1995; Alcalá et al., 2013a; *and references therein*). In smectite-rich environments (as the SP, PC, and SC successions), the comparison of smectite and kaolinite vs. illite ((S + K):I) changes with the global sea-level curves and enables to identify the influence of the global eustasy (Clark et al., 2009; Daoudi et al., 1995), and local tectonics (Jamoussi et al., 2003; Martín-Martín et al., 2001). A low diagenetic overprint is needed for using the temporal distribution of clay-mineral assemblages (Alcalá et al., 2013b, 2013a, 2001; Ruffell et al., 2002). The presence of smectite (and mixed layer I-S) in all SP, PC, and SC successions indicates weak burial diagenesis because this mineral phase is quite sensitive to temperature rise with burial depth, and tends to disappear above 200°C after an exponential rate of illitisation between 120°C and 150°C (Lanson, Sakharov, Claret, & Drits, 2009; Nadeau & Bain, 1986). The dimensionless (S + K):I ratio varies in the 1.21–2.17 range in the SC, in the 0.75–2.76 range in the PC, and in the 0.40–1.39 range in the SP successions (Figure 3), thus suggesting a more proximal sediment supply in SP (both in the Congost, Lower Tap, and Upper Tap Formations) than in the corresponding SC and PC successions.

The arenite petrography indicates that the prevalent component in all the studied successions are siliciclastics and carbonates (Table 5; Figure 7). The SC and PC successions are characterized by arenites (quartzarenites, sub-litharenites, litharenites, and bio-calcarenites) and limestones (siltstones, mudstones, and packstones). The SP successions are characterized by clastic rocks (litharenites, sub-litharenites, and bio-

Table 3. Significant species assemblages of planktonic foraminifera of samples from Sierra del Carche, Pinoso Corridor, and Sierra de la Pila sectors.

AREAS	LOGS	FORMATIONS	LITHOFACIES	SAMPLES	Globigerina bulloides d'Orbigny	Globoturborotalita woodi (Jenkins)	Globoturborotalita druryi (Akers)	Globoturborotalita nepenthes (Todd)	Globigerinoides subquadratus (Brönnimann)	Globigerinoides obliquus Bolli	Globigerinoides extremus Bolli & Bermúdez	Globigerinoides trilobus (Reuss)	Globigerinoides bisphaericus Todd	Praeorbulina sicanus (De Stefani)	Praeorbulina glomerosa (Blow)	Orbulina suturalis Brönnimann	Orbulina universa d'Orbigny	Globigerinella obesa (Bolli)	Globigerinella siphonifera (d'Orbigny)	Paragloborotalia siakensis (LeRoy)	Paragloborotalia acrostoma (Wezel)	Neogloboquadrina continuosa (Blow)	Neogloboquadrina acostaensis (Blow)	Neogloboquadrina humerosa (Takayanagi & Saito)	Globorotalia peripheroronda Blow & Banner	Globorotalia peripheroacuta Blow & Banner	Globorotalia scitula (Brady)	Globorotalia miozea (Finlay)	Globorotalia praemenardii Cushman & Stainforth	Globorotalia menardii (Parker, Jones & Brady)	Globorotalia plesiotumida Blow & Banner	Globigerinita glutinata (Egger)	Turborotalita quinqueloba (Natland)	Globoquadrina baroemoenensis (LeRoy)	Globoquadrina globosa Bolli	Globoquadrina langhiana (Cita & Gelati)	Globoquadrina dehiscens (Chapman, Parr & Collins)	NEOGENE ZONES (Blow, 1969)	AGE

(This is a very large data matrix with species occurrence marks "o" arranged by sample across the sectors Sierra de la Pila (1. Barranco El Mulo, 2. Estación Blanca, 3. El Buitre, 4. Umbria Moreno), Sierra del Carche (5. Barranco Pardinas), and Pinoso Corridor / SC (6. La Alberquilla).)

1. Barranco El Mulo — Lower Tap Fm / Congost Fm

Lithofacies	Sample	Zone	Age
H	P49	N10	Late Langhian
H	P48	N10	Late Langhian
H	P47	N10	Late Langhian
H	P46	N10	Late Langhian
G	P45	N9	Late Langhian
G	P44	N9	Late Langhian
G	P43	N8	Early Langhian
G	P41	N8	Early Langhian
G	P40	N8	Early Langhian
G	P39	N8	Early Langhian
D (Congost Fm)	P38	N8	Early Langhian
D (Congost Fm)	P37	N8	Early Langhian

2. Estación Blanca — Lower Tap Fm / Congost Fm

Lithofacies	Sample	Zone	Age
H	P63	N10	Late Langhian
G	P62	N9	Late Langhian
G	P61	N9	Late Langhian
G	P60	N9	Late Langhian
G	P59	N9	Late Langhian
G	P58	N9	Late Langhian
G	P57	N9	Late Langhian
G	P56	N9	Late Langhian
G	P55	N9	Late Langhian
F (Congost Fm)	P53	N9	Late Langhian
F (Congost Fm)	P52	N8	Early Langhian
D	P51	N8	Early Langhian

3. El Buitre — Lower Tap Fm

Lithofacies	Sample	Zone	Age
G	Pila 12	N10	Earliest Serravallian
G	Pila 11	N10	Earliest Serravallian
G	Pila 10	N10	Earliest Serravallian
G	Pila 9	N10	Earliest Serravallian
G	Pila 13	N9	Late Langhian
G	Pila 14	N9	Late Langhian

4. Umbria Moreno — Lower Tap Fm

Lithofacies	Sample	Zone	Age
G	Pila 8	N9	Late Langhian
G	Pila 7	N9	Late Langhian
G	Pila 3	N8	Early Langhian
G	Pila 4	N8	Early Langhian
G	Pila 5	N8	Early Langhian
G	Pila 6	N8	Early Langhian

5. Barranco Pardinas (Sierra del Carche) — L Tap Fm / Congost Fm

Lithofacies	Sample	Zone	Age
G	C28	N8	Early Langhian
G	P6	N8	Early Langhian
G	P5	N8	Early Langhian
G	P4	N8	Early Langhian
D	C27	N8?	Early Langhian?
C	C25	N7-N8	Earliest Langhian – Latest Burdigalian
C	C24	N7-N8	No planktonic foraminifera
C	P3	N7-N8	Earliest Langhian – Latest Burdigalian
C	P2	N7-N8	Earliest Langhian – Latest Burdigalian
C	C23	N7-N8	No planktonic foraminifera
C	P1	N7-N8	Earliest Langhian – Latest Burdigalian

6. La Alberquilla (Pinoso Corridor / SC) — Upper Tap Fm / Lower Tap Formation / Congost Fm

Lithofacies	Sample	Zone	Age
R	C50	N17	Late Tortonian
R	C49	N17	Late Tortonian
R	C48	N16	Middle Tortonian
N	C44	N13	Late Serravallian
N	C43	N13	Late Serravallian
N	A18	N12	Late Serravallian
N	A17	N12	Late Serravallian
N	C41	N12	Late Serravallian
N	C40	N12	Late Serravallian
N	A16	N11	Early Serravallian
N	A15	N11	Early Serravallian
N	A14	N11	Early Serravallian
N	A13	N11	Early Serravallian
L	A12	N10	Late Langhian
L	A11	N10	Late Langhian
L	A10	N10	Late Langhian
L	A9	N10	Late Langhian
L	C39	N9	Late Langhian
L	A8	N9	Late Langhian
L	A7	N9	Late Langhian
L	A6	N8	Early Langhian
L	A5	N8	Early Langhian
L	A4	N8	Early Langhian
L	A2	N8	Early Langhian
L	C37	N8	Early Langhian
L	A1	N8	Early Langhian
J	C35	N8	Early Langhian
H	C32	N8	Early Langhian
H	C31	N8	Early Langhian
H	C30	N8	Early Langhian

Table 4. Average whole-rock and clay-fraction mineralogy (in wt. %) of samples from Sierra del Carche (SC), Pinoso Corridor (PC), and Sierra de la Pila (SP) sectors (Qtz, quartz; Cal, calcite; Dol, dolomite; Phy, phyllosilicates; Kfs, K-feldspar; Pl, plagioclase; Gp, gypsum; Sme, smectite; Ill, illite; I-S, mixed layer illite-smectite; and Kln, kaolinite), and the dimensionless (smectite+ kaolinite): illite ((S + K):I) ratio.

Sector	Log	Formation	Lithofacies, Age	Sample	Whole-rock mineralogy							Clay-fraction mineralogy				(S + K):I ratio
					Qtz	Cal	Phy	Dol	Kfs	Pl	Gp	Sme	Ill	I-S	Kln	
PC	Log 6	Upper Tap Formation	R, middle Tortonian	C50	5	37	32	12	6	< 5	6	29	52	9	10	0.75
				C49	5	40	25	13	8	< 5	7	33	48	5	14	0.98
				C48	5	31	27	19	7	< 5	8	44	33	9	14	1.76
		Lower Tap Formation	N, upper Serravallian	C44	< 5	43	22	17	6	< 5	6	48	25	6	21	2.76
				C43	5	45	21	13	7	< 5	7	36	29	15	20	1.93
			N, lower Serravallian	C41	5	50	21	11	5	< 5	6	39	24	16	21	2.50
				C40	< 5	43	24	19	< 5	< 5	< 5	44	29	13	14	2.00
			L, upper Langhian	C39	5	39	30	10	7	< 5	6	57	29	8	6	2.17
SC			H, J, lower Langhian	C37	< 5	46	25	10	6	5	5	56	30	6	6	2.07
				C35	6	43	29	7	8	< 5	5	54	32	11	< 5	1.78
				C32	< 5	28	29	23	< 5	7	5	41	36	6	17	1.61
				C31	< 5	34	30	15	5	7	5	46	34	8	12	1.71
				C30	8	20	30	30	6	6		33	43	7	17	1.16
	Log 5	Lower Tap Formation	G, lower Langhian	C28	6	58	18		6	8	< 5	42	39	14	5	1.21
		Congost Formation	C, D, lower Langhian	C27	6	38	29	14	5	8		40	41	5	14	1.32
				C25	5	55	20	6	6	8		52	33	12	< 5	1.67
				C24	< 5	37	27	7	9	10	6	44	36	15	5	1.36
			C, upper Burdigalian	C23	9	41	30	5	8	7		37	46	11	6	0.93
SP	Log 2	Lower Tap Formation	H, lower Serravallian	P64	7	64	14	10	5			21	50	25	< 5	0.50
			G, H, I, upper Langhian	P63	11	45	19	11	10	< 5		22	62	11	5	0.44
				P62	12	44	22	13	5	< 5		17	65	6	12	0.45
				P61	6	71	17	6				16	62	7	15	0.50
				P60	9	46	23	22				20	59	< 5	17	0.63
				P59	8	50	23	19				22	55	11	12	0.62
				P58	12	61	8	19				16	58	19	7	0.40
				P57	20	49	24	7				21	55	19	5	0.47
				P56B	8	48	26	18				29	52	8	11	0.77
				P56A	9	58	17	16				46	38	9	7	1.39
		Congost Formation	D, F, lower Langhian	P55	8	65	8	19				23	59	10	8	0.53
				P53 a	7	59	< 5	33								
				P52	< 5	60	8	30				41	40	10	5	1.15
				P51 a	8	83	< 5	8								
	Log 1	Lower Tap Formation	H, upper Langhian	P49	7	55	20	18				30	44	18	8	0.86
				P48	10	33	12	35	10			33	44	16	7	0.91
				P47	5	45	24	19		7		33	43	16	8	0.95
				P46	5	42	23	21	9			31	41	21	7	0.93
				P45	6	47	31	16				26	38	20	16	1.11
				P44	7	45	25	16	7			34	37	21	8	1.14
			G, lower Langhian	P43	< 5	34	31	23	8			41	40	14	5	1.15
				P41	6	51	27	10	6			38	37	17	8	1.24
				P40	5	53	23	19				34	39	15	12	1.18
				P39	8	47	27	18				36	47	10	7	0.91
		Congost Formation	D, lower Langhian	P38	< 5	80	16					39	39	16	6	1.15
				P37	< 5	84	14					34	44	17	5	0.89

calcarenites). The fossil assemblage contained in the bio-calcarenites consists of larger foraminifera, Bryozoa, coralline red algae, planktonic foraminifera, and echinoderms. Bio-calcarenites show symmetrical cement rims (isopachous) consisting of microcrystalline crystals developed around bioclasts.

Information deduced from reworked clasts identifies whitish marls and turbiditic arenites of probable Cretaceous-Paleogene origin in most of the studied samples. Both in the SC, PC, and SP successions, inherited calcite and dolomite grains combines with neo-formed dolomite- and calcite-rich cement rims (Table 5). As described by Alcalá et al. (2013b) and Martín-Martín et al. (2018b) in comparable Miocene Subbetic successions, calcite and dolomite come from a combination of neo-formation processes in lacustrine and internal platform realms and detrital supplies from source areas. These realms are marked by warm and shallow water under certain thermodynamics conditions and abundance of base cations, and detrital supplies from a given source area in variable (usually unknown) proportions. Reworked (and probably weathered) Triassic reddish clays and gypsum appear systematically in Lithofacies P (Log 4) and O (Log 2, P65) in the SP successions. The whole-rock mineralogy has identified this inherited Triassic influence in studied Lithofacies in the PC and CS successions. See Tables 1 and 5 for further details on Lithofacies and petrography.

5. Discussion

5.1. Depositional sequences and sedimentary realms

The stratigraphic record is characterized by a Miocene *p.p* sedimentary cycle that: (1) encompasses the Congost Formation (upper Burdigalian-upper Langhian *p.p.*) and the Lower and Upper Tap Formations (upper Langhian
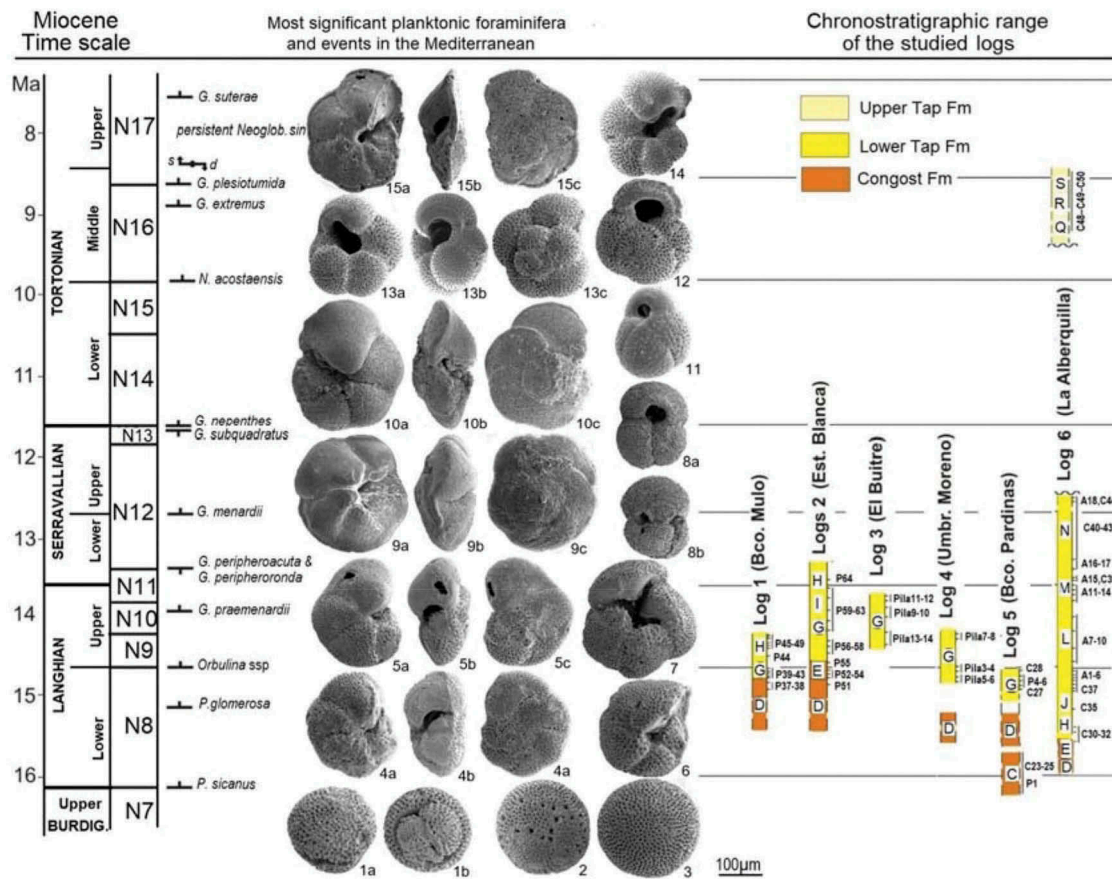
Figure 5. Miocene chronostratigraphy of the studied successions based on planktonic foraminifera assemblages. Significant planktonic foraminifera represented: 1.-*Praeorbulina sicanus* (De Stefani); log 6, sample C31. 2.- *Orbulina suturalis* Brönnimann; log 6, sample A8. 3.- *Orbulina universa* d'Orbigny; log 6, sample A8. 4.- *Globorotalia peripheroronda* Blow & Banner; log 6, sample C37. 5.- *Globorotalia peripheroacuta* Blow & Banner; log 6, sample A14. 6.- *Globoquadrina dehiscens* (Chapman, Parr & Collins); log 6, sample A7. 7.- *Globoquadrina langhiana* (Cita & Gelati); log 6; sample A1. 8.- *Globigerinoides subquadratus* (Brönnimann); log 6, simple A2. 9.- *Globorotalia praemenardii* Cushman & Stainforth; log 6, sample A11. 10.- *Globorotalia menardii* (Parker, Jones & Brady); log 6, sample C40. 11.- *Globoturborotalita nepenthes* (Todd); log 6, sample C49. 12.- *Globigerinoides extremus* Bolli & Bermúdez; log 6, sample C49. 13.- *Neogloboquadrina humerosa* (Takayanagi & Saito) rigth-coiling; log 6, sample C49. 14.- *Neogloboquadrina humerosa* (Takayanagi & Saito) left-coiling; log 6; sample C 50. 15.- *Globorotalia plesiotumida* Blow & Banner; log 6, sample C49.

p.p.-upper Tortonian); (2) is bounded by two main unconformities related to emersion periods and/or tectonic deformation events and referable to the late Burdigalian and late Tortonian, respectively (Figure 8); and (3) lies unconformably above the Paleogene to Aquitanian *p.p.* cycle (Miñano and Murtas Formations); and (4) is covered by the Plio-Quaternary *p.p.* depositional one. The analyzed succession (Figure 8) fits with the Main Cycle VII proposed by Vera (2000, 2004). An erosive boundary divides the sedimentary cycle into the upper Burdigalian-upper Serravallian and middle Tortonian depositional sequences: (1) the oldest shows a transgressive-regressive trend with a maximum flooding surface dated upper Langhian; and (2) the upper sequence shows a regressive trend only. The whole cycle shows a transgressive to regressive depositional trend with several secondary fluctuations reflected by parasequences. Lithofacies, mineralogy (including (S + K):I ratios), and petrography evidence shallower environments in SP than in SC and PC sectors.

(1) The upper Burdigalian-upper Serravallian Depositional Sequence displays a transgressive-regressive trend (Guerrera & Martín-Martín, 2014a). The transgression begins in the upper Burdigalian (Lithofacies C), reaches the late Langhian (Lithofacies L, G, H, and I), and seems younger in Log 6 (early Langhian, Lithofacies D) than in Log 5 although the different age might be related to an onlap arrangement of transgressive deposits on the previous deformed substratum (Figure 8). The occurrence of an internal platform environment marked by warm and shallow water during the early Langhian in both the SC and SP sectors is suggested by lithofacies association, lower (S + K):I ratios, calcite and dolomite neo-formation, and fossil assemblages. The transition to arenites in the upper part of the early Langhian (Table 5) marks the occurrence of a mixed carbonate and terrigenous input that is consistent with the evolution to an external platform to upper slope. Data allowed proposing for the Congost Formation a deposition occurring in lagoon to upper slope environments.
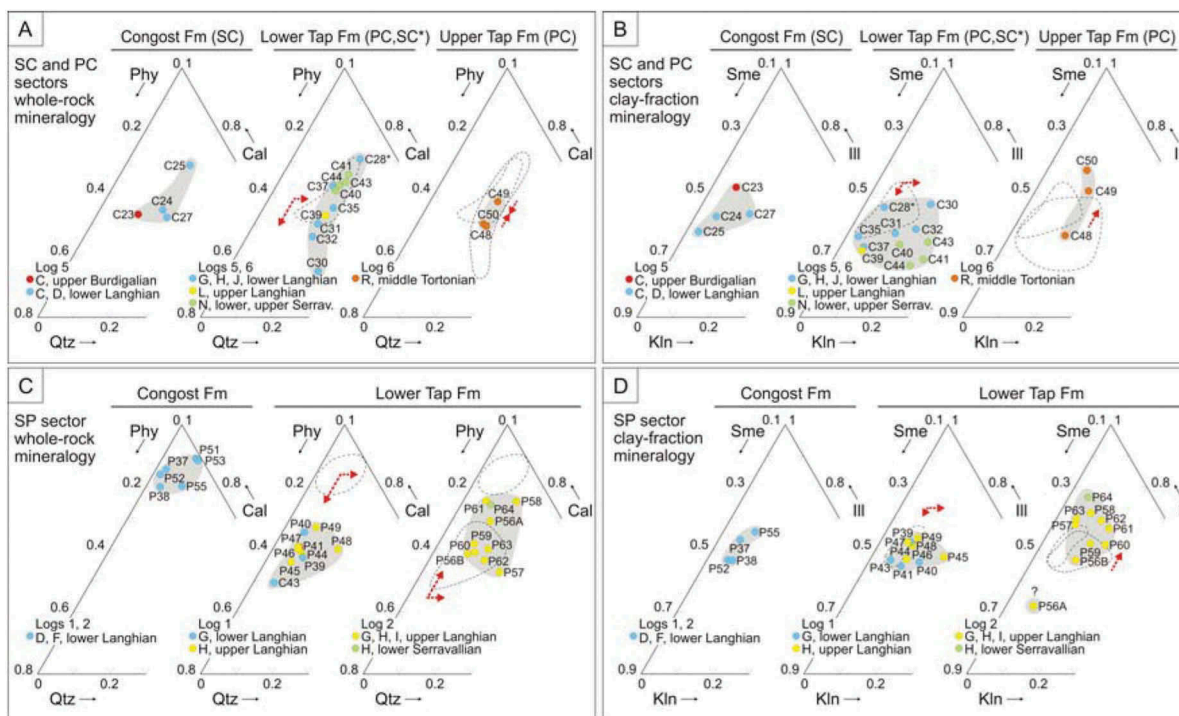
Figure 6. Ternary plots for whole-rock (A and C) and clay-fraction (B and D) mineralogical associations from the Sierra de El Carche (SC), Pinoso Corridor (PC), and Sierra de La Pila (SP) successions. Data clustered by sector, formation and Log as in Figure 3 and Table 4 (Qtz, quartz; Cal, calcite; Phy, phyllosilicates; Sme, smectite; Ill, illite; and Kln, kaolinite). The red dotted lines within the plots show the temporal dynamics of the mineral assemblages.
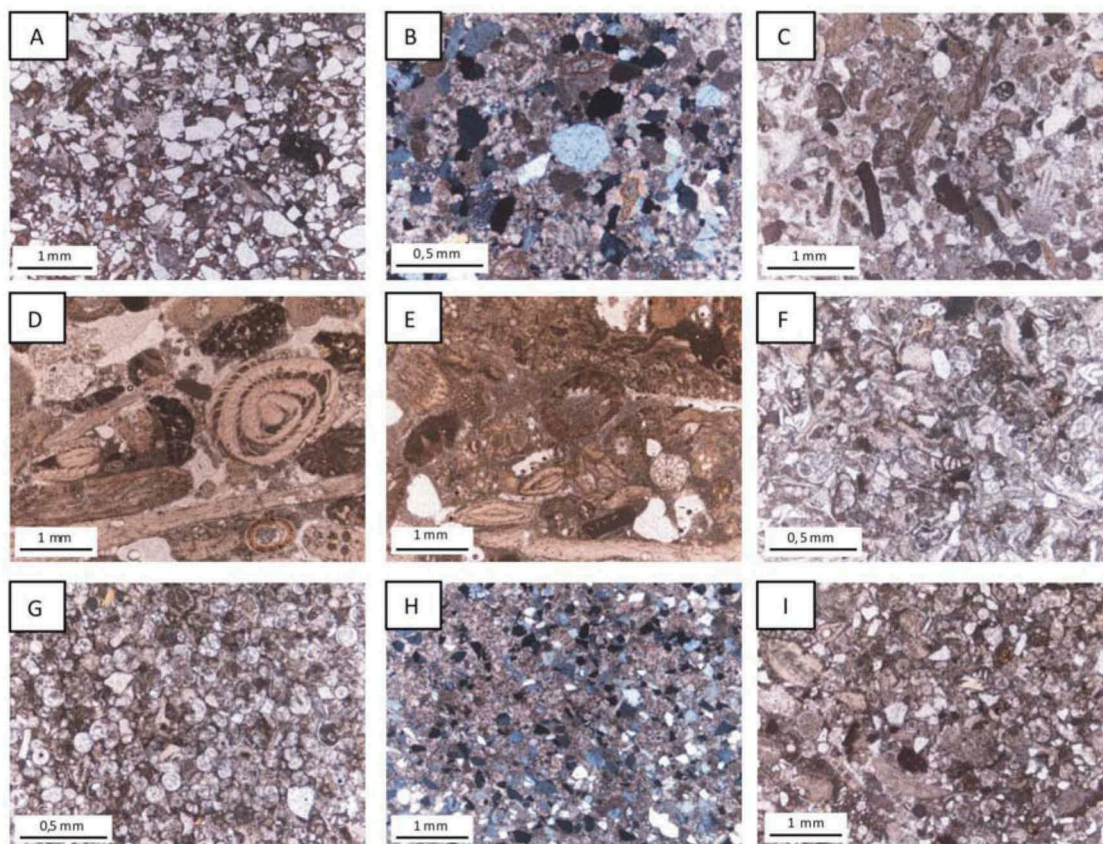

Figure 7. Photomicrographs of representative lithotypes of the Sierra de El Carche (A and B), Pinoso Corridor (C to E), and Sierra de La Pila (F to I) successions. (A) Quartzarenite, sample C34, plane-polarized light (PPL); (B) litharenite, sample C36, cross-polarized light (CPL); (C) biocalcarenite, sample C38, PPL; (D) bioclastic packstone, sample C45, PPL; (E) bioclastic packstone, sample C46, PPL; (F) biocalcarenite, sample P36, PPL; (G) biocalcarenite, sample P42, PPL; (H) sub-litharenite, sample P50, CPL; and (I) litharenite, sample P54, PPL.

Table 5. Synthetic description of petrofacies in thin sections of samples from Sierra de El Carche (SC), Pinoso Corridor (PC), and Sierra de La Pila (SP).

Log Sector	Sample	Lithofacies	Unit (age)	Petrofacies	Description
6 (PC)	C51	S	**Upper Tap Formation** (middle Tortonian)	Litharenite	As sample C36
	C47	Q		Bioclastic packstone	Skeletal fragments of larger foraminifera, Bryozoa, Echinoid spines, and coralline red algae. Some crystals of monocrystalline quartz (rarer polycrystalline). Intergranular space filled by sparite cement.
	C46			Bioclastic packstone	As sample C47
	C45			Bioclastic packstone	As sample C47
	C42	N	**Lower Tap Formation** (upper Serravallian)	Biomicritic limestone (mudstone)	Sponge spicules. Low amount (1–2 vol. %) of quartz, K-feldspar, plagioclase, and organic fragments.
	C38	L	**Lower Tap Formation** (upper Langhian)	Bio-calcarenite	Prevalent carbonatic rock fragments (mainly mudstones, rarely wackestones), and bioclasts of planktonic foraminifera, Bryozoa, and coralline red algae. Low amount of mono- and poly-crystalline quartz. Cement supported. Two types of calcite cement: very fine-grained bounding the clasts and druzy mosaic filling pores.
6 (SC)	C36	J	**Lower Tap Formation** (lower Langhian)	Litharenite	Angular monocrystalline quartz, abundant rock fragments (mudstones and wackestones) and skeletal clasts, rare polycrystalline quartz, K-feldspar, and glauconia. Bioclasts are mainly foraminifera both benthic (Miliolids) and lesser of planktonic. Poorly sorted with a medium-grained class of about 300 μm: a fine-grained fraction of about 100 μm and coarser bioclasts reaching about 700 μm. Intergranular spaces are filled by sparry cement, while no matrix was found. Syntaxial overgrowth of calcite cement on rock fragments (in optical continuity).
	C34			Quartz-arenite ($Q_{96} F_{2.5} L + C_{1.5}$)	Angular crystals of mono- and poly-crystalline quartz, carbonatic rock fragments (mudstones/wackestones, and sparites), bioclastic fragments (e.g. benthic larger and planktonic foraminifera, coralline red algae, and individual component of echinoderm stalks and spines), chert, mica flakes (mainly muscovite), K-feldspars, plagioclase, and glauconite. Bad-sorted. The average clast size is about 250 μm, with exception of skeletal fragments that reach almost 1 mm. Grains are cemented by sparite. Symmetrical cement rims (isopachous) around grains consisting of microcrystalline crystals; micrite as a matrix is found; siliceous cement (chalcedony) is also within bioclasts.
	C33	H		Bio-calcarenite	As samples C29
	C29	E	**Congost Formation** (lower Langhian)	Bio-calcarenite	Bioclasts and unbroken fossils (e.g. planktonic foraminifera) and minor amount of angular quartz crystals, carbonatic (calcite and dolomite) rock fragments, and rare biotite. Very fine-grained. Grain-supported.
5 (SC)	C26	D		Siltstone	Crystals of quartz, bioclasts, carbonatic fragments (almost all sparitic) and rare thin colorless mica flakes (muscovite).
2 (SP)	P54	F	**Congost Formation** (lower Langhian)	Litharenite	Mono- and poly-crystalline quartz (mainly angular), carbonatic rock fragments (micritic and sparitic) and bioclasts (planktonic foraminifera, larger foraminifera, Briozoa, etc.), rare dolomite, K-feldspar, and plagioclase. Carbonatic cement and matrix. The average grain size is about 200 μm, with exception of bioclastic fragments reaching 3.5 mm diameter.
1 (SP)	P50	H	**Lower Tap Formation** (upper Langhian)	Sub-litharenite	Angular mono- and poly-crystalline quartz, carbonatic rock fragments (sparitic and micritic), bioclasts, and rare K-feldspar, plagioclase, and muscovite. Grain size is about 250 μm. Both carbonatic cement and matrix.
	P42	G		Bio-calcarenite	Almost totally made up of planktonic foraminifera with inner chambers filled by carbonatic cement.
	P36	D	**Congost Formation** (lower Langhian)	Bio-calcarenite	Several bio-skeletal fragments, unbroken fossils of benthic foraminifera (Miliolids), and minor amount of planktonic foraminifera and echinoids. Crystals of quartz and plagioclase in very low quantities. All clasts are cemented by sparite-microsparite.

The Congost Formation passes laterally and upward into the Lower Tap Formation. The presence of clastic rocks suggests a transition from a platform to a basinal environment marked by a terrigenous supply. So, according to the sedimentological data above exposed, the Lower Tap Formation represents the sedimentation on an external carbonate platform to upper slope realms (Lithofacies G, J, and H) changing upward to deeper basinal conditions (Lithofacies I, L, and N). Lateral variations of these two formations are probably related to a different age of the Congost Formation top, that is lower Langhian *p.p* (lower part) in SC (Logs 5, 6) and lower Langhian *p.p.* (upper part)-upper Langhian *p.p.* in SP (Logs 1, 2, 4). This lateral diachronism may be caused by variations in the local paleogeography. The Lower Tap Formation shows deeper marine lithofacies in SC than in SP with a quartzarenitic supply (Lithofacies J) in SC that is missing in the SP sector. The deepest environment is marked by the upper Langhian *p.p.* Lithofacies I (silexites; Log 2) (Bally & Snelson, 1980). In turn, the presence of slumps in the SC (Lithofacies M) implies a slope environment (Bosellini, Mutti, & Ricci-Lucchi, 1989). Both silexites and slumps are considered to indicate a maximum flooding surface. The presence of fine-grained deposits in the SC during the upper Serravallian may indicate a more open pelagic and distal environment (Figure 3).
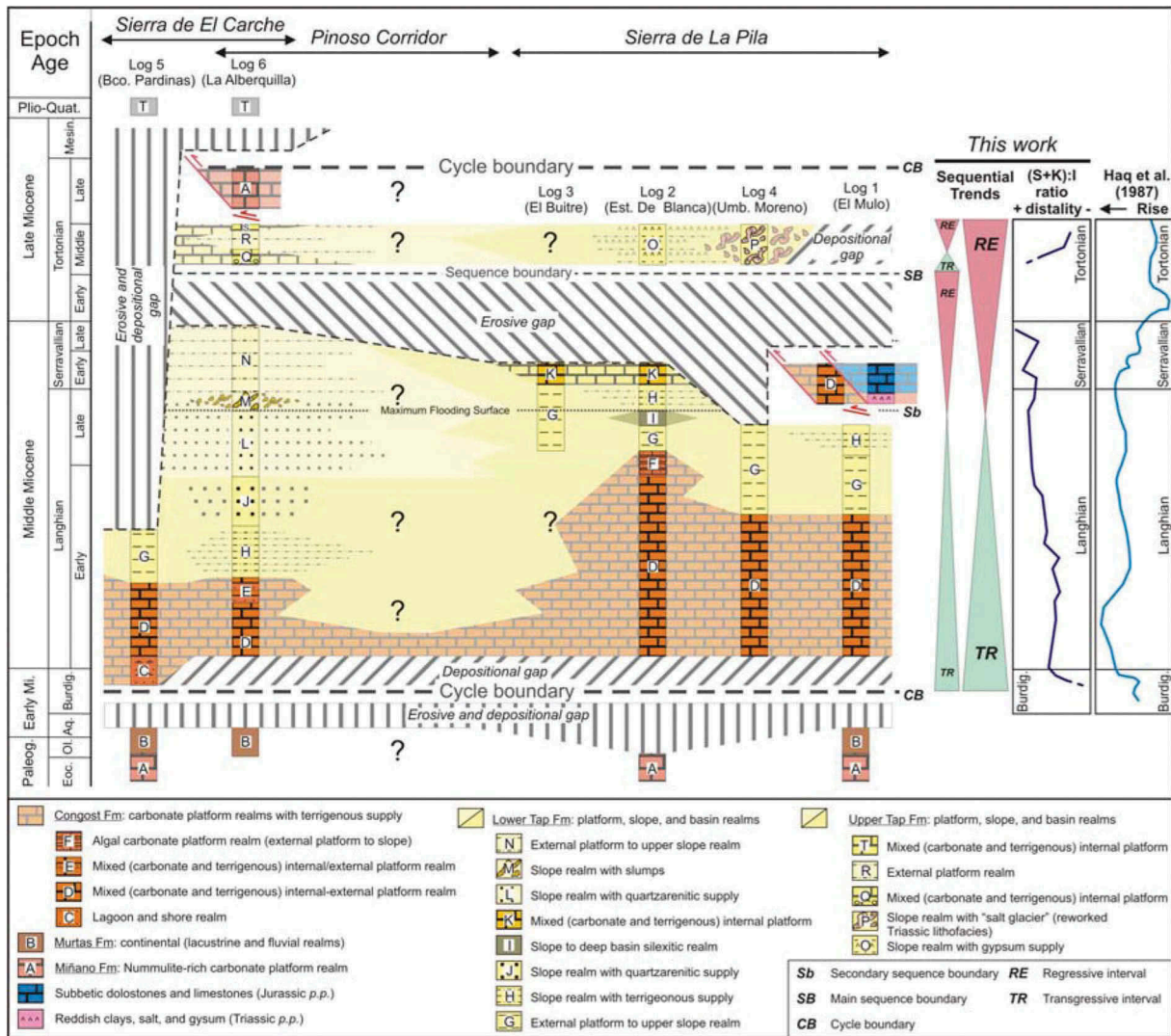
Figure 8. Depositional sequences, and vertical and lateral lithofacies variations resulting from the stratigraphic architecture reconstructed through interdisciplinary analyses of the studied successions. Stratigraphic gaps and associated unconformities are interpreted as non-depositional and/or erosive phases. Depositional trends recognized from the facies evolution and their comparison with the synthetic local relative sea-level curve deduced from the dimensionless (S + K):I ratio and the global sea-level curve from Haq et al. (1987) are reported. The main and secondary transgressive and regressive trends are also indicated.

At the end of this depositional sequence, the main latest Serravallian *p.p.*-Tortonian *p.p.* 3 Ma gap recorded in the study area was probably related to a local/regional regression that leads to an emersion at the beginning of the compressional thin-skinned tectonics. A similar situation has been recently mentioned for the eastern External Betic Zone in the Alicante area (Martín-Martín et al., 2018a, 2018b) where a gap related to compressional tectonics has been proposed affecting the Langhian-Serravallian *p.p.* In the study area, this tectonics was pre-dated both by compression and folding and by lithostatic load of the Sierra de La Pila Nappe. So that, subsiding areas developed in the PC sector while uplifting areas took place in the SP and SC sectors. This assertion is corroborated by the thicknesses of the Langhian-Serravallian successions in these sectors (higher in the PC, and lower in the SP and SC sectors, respectively).

(2) The Middle Tortonian Depositional Sequence is a new transgressive-regressive depositional sequence

deposited above the former unconformity, and represented by the Upper Tap Formation well exposed in the SC and PC (Log 6). According to the sedimentological data above exposed, in these sectors this sequence deposited on internal mixed (carbonate and siliciclastic) platform (Lithofacies Q and S) to external platform (Lithofacies R) environments. In the middle Tortonian after the initial transgression, calcite and smectite decrease, and detrital minerals such as quartz, K-feldspar, plagioclase, illite, and kaolinite increase (Table 4; Figure 6(A,B)), thus indicating a new relative sea-level fall and sediment reworking (Figure 3).

In the SP sector an equivalent unconformity has been recognized above the Lower Tap Formation. Above this unconformity, the Lithofacies O and P belonging to the Upper Tap Formation have been found. In spite of that, no biostratigraphically significant fauna has been found and so the age attribution

for these levels was inferred. This sequence shows the supply of reworked clays and gypsum from the erosion of Triassic terrains and is thought to be deposited on a slope realm (Lithofacies O and P) by the presence of olisthostromes. Equivalent deposits have been described recently in the eastern External Betic Zone from the Alicante area and assigned to the late Miocene (Martín-Martín et al., 2018a, 2018b). In this sector this sequence is unconformably followed by the Pliocene-Quaternary succession (Lithofacies T).

5.2. Tectonic control on sedimentation

The Miocene syn-sedimentary tectonic activity is evidenced by:

(1) Lithofacies record a variable terrigenous supply, indicating the uplift of source areas, a shallower platform sedimentation, and the decrease of distality (lower (S + K):I values) evidencing a short transport (appearance of angular quartz grains). The Congost Formation is composed mainly of carbonate rocks while arenites predominates regarding carbonates in the Lower and Upper Tap Formations. The terrigenous component of both formations is made up mainly of angular quartz grains, bioclasts and/or carbonate fragments, and minor amounts of K-feldspar, plagioclase, micas (biotite and muscovite), glauconia, dolomite, and chert. Reworked (and probably weathered) Triassic reddish clays and gypsum grains appear systematically in the SC, PC, and SP sectors. Arenites of the Lower Tap Formation in the SC sector are quartz-richer. Rock fragments (mostly carbonatic) are more abundant in the SP sector. A minor amount of carbonate fragments could be attributed to a longer transport for the SC with respect to the SP. Relationships between source/basin areas are also thought to be controlled by tectonics. Taking the former tectonic alignments and the south-to-north migrating deformation into account, a southern main rising source area including mainly Cretaceous and Paleogene terrains, and Triassic materials to a lesser extent is proposed, as deduced from the clay-mineral association, presence of detrital gypsum, K-feldspar, and plagioclase, and the planktonic foraminifera reworking.

(2) Frequent syn-sedimentary upper Langhian slumps in the Lower Tap Formation in the SC (Log 6) indicate a pronounced tectonic activity characterized by sliding of unconsolidated materials in a slope environment. These 'tectofacies' predate a local regression that leads to an emersion occurring during the latest Serravallian and probably related to the beginning of the thin-skinned tectonics. A second 'tectofacies' from the Upper Tap Formation consisting of middle Tortonian olistostromes of reworked Triassic material was observed in the SP sector. Tent-Manclús, Estévez, and Martín-Martín (2000; and references therein) interpreted these deposits as olithostrome-like or 'salt glacier' deposits. In the eastern External Betics the salt glaciers are related to overflow of Triassic clays and gypsum from the basal level of stacked superficial nappes or from diapirs (Martín-Martín et al., 2018a, 2018b). In the SP sector, this event appears to be contemporaneous with the emplacement of the Subbetic Nappe, despite a continuous minor supply of reworked (and probably weathered) Triassic terrains and seems to extend over the whole Miocene record, as deduced from mineralogical and petrographic data.

(3) Lithofacies thicknesses and lateral changes (Figure 8) are also thought to be related to paleogeographic changes due to tectonics. In particular, the SC sector shows greater sedimentary thicknesses, indicating a greater subsidence. Conversely the studied SP successions are thinner. Also the Congost Formation (internal platform) is thicker in the SC indicating a low subsiding area. A similar sedimentary evolution characterizes the deeper Lower and Upper Tap Formations, which show the thickest and deepest deposition in the SC and the thinnest and shallowest deposition in the SP sector. Nevertheless, during the late Langhian this trend is inverted and deeper silexitic facies in the SP indicate a deepening regarding the SC.

(4) The comparison of the (S + K):I ratio changes (synthetic local sea-level curve) with the global sea-level curve of Haq, Hardenbol, and Vail (1987) enabled to deduce the influence of global eustasy (Daoudi et al., 1995; Clark et al., 2009; Alcalá et al., 2013a) and local tectonics (Martín-Martín et al., 2001; Jamoussi et al., 2003; Alcalá et al., 2013a) on the SC, PC, and SP successions (Figure 8). For a common sampling density, such as in this study, the (S + K):I ratio allowed drawing the global sea-level cycles defined by Haq et al. (1987) and to propose local tectonics as the cause of divergences defining low-order cycles during the Langhian and especially during the Serravallian.

5.3. Tectono-sedimentary evolutionary model

An evolutionary Miocene paleotectonic framework is presented in four steps and discussed below (Figure 9). In the early Miocene the area was affected by a blind thrusting and related gentle folds (Figure 9(A)).

(1) Burdigalian p.p.-Langhian p.p. (Figure 9(B)). An internal platform (Congost Formation) transitionally develops upwards to an external platform realm (Lower and Upper Tap Formations). The progressive deformation could produce vertical and lateral lithofacies variations and environmental changes from the Congost Formation to the Lower Tap Formation. Main thrusts are thought to display a transpressive dextral strike-slip displacement related to the SW-NE orientation of these faults regarding the W-E to NW-SE
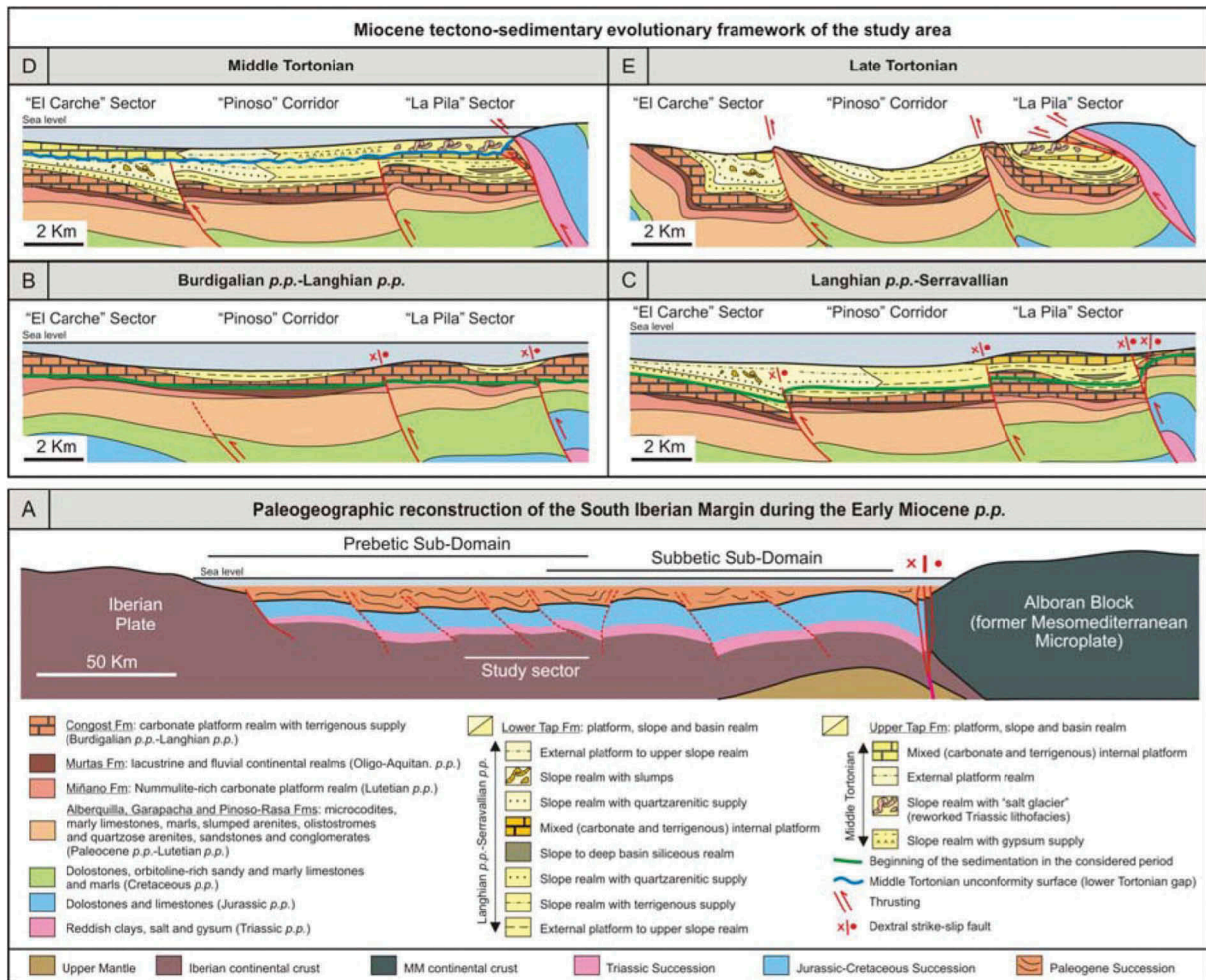
Figure 9. Reconstruction of the paleogeographic and paleotectonic evolution of the area. (A) Paleogeographic sketch showing the South Iberian Margin during the early Miocene; and (B to E) Paleotectonic deformation model of the External Betic Zone (Prebetic-Subbetic transition) represented in four steps: (B) Burdigalian *p.p.*-Langhian *p.p.*; (C) Langhian *p.p.*-Serravallian; (D) middle Tortonian; and (E) late Tortonian.

maximum compressive stress axis. This evolution could cause the development of gentle synclines and anticlines in areas between strike-slip faults (cf. Figure 2).

(2) Langhian *p.p.*-Serravallian (Figure 9(C)). A great variety of hemipelagic, platform, and slope deposits developed in the Lower Tap Formation. Marked differences in the subsidence rate are interpreted as due to the reactivation of faults and progressive syn-sedimentary folding. During this time span main thrusts are characterized by a transpressive dextral strike-slip displacement related to a NW-SE oriented maximum compressive stress. The occurrence of the deepest environment (slope) in the synclines of the PC and SP is indicated by siliceous deposits and a large terrigenous supply with a slump interval developed in the uppermost Langhian, probably due to uplifting of source areas.

(3) Middle Tortonian (Figure 9(D)). The platform sedimentation settled (Upper Tap Formation) and a subsidence inversion occurred since the SC sector is transformed into a rising area with the development of an internal platform zone. On the other hand, in the SP sector olisthostrome-like and/or 'salt glacier' deposits fed

by Triassic terrains developed. The main faults are now thought to display only a reverse movement according to a N-S oriented maximum compressive stress. The beginning of the Subbetic Nappe emplacement above the SP should occur in this period generating a tectonic load in the SP that caused a deepening of this area, the rising of the SC, and the extensive supply of Triassic material into the basin.

(4) Late Tortonian (Figure 9(E)). No sedimentation was verified, and in the SC-PC boundary the emergence of thrusts affecting the upper deposits (Log 6) occurred. These factors caused the complete emplacement of the Subbetic Nappe to override the upper sediments of the SP sector due to N-S compression (De Ruig, 1992; Sanz De Galdeano & Buforn, 2005).

5.4. Lateral correlations and geodynamic implications

In this section we present: (1) a central-western Mediterranean paleogeographic-geodynamic interpretative framework (Figure 10(A)), as developed and discussed by Guerrera and Martín-Martín (2014b; *and*
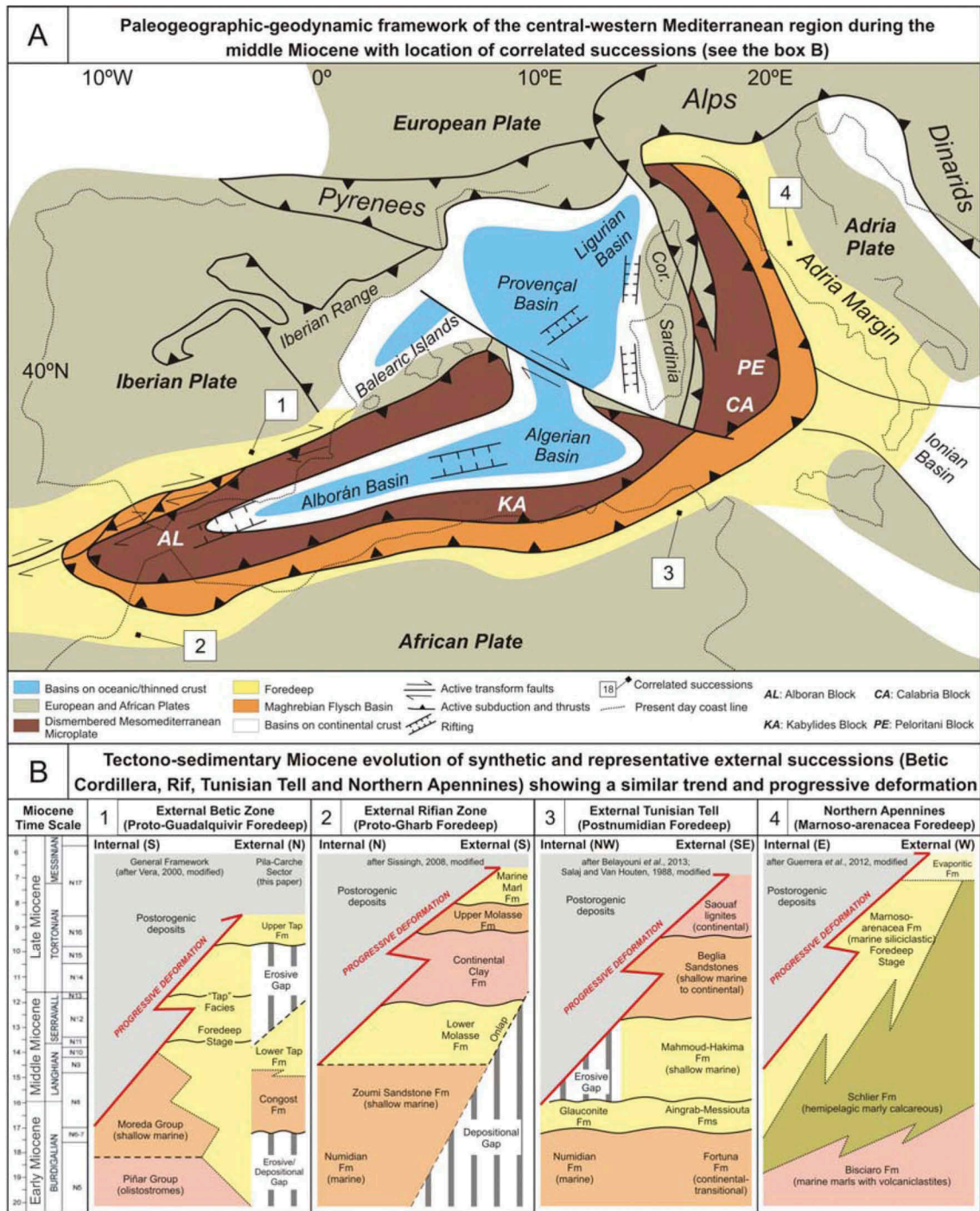
Figure 10. (A) Paleogeographic-geodynamic model of the western Mediterranean showing the Apennine-Maghrebian Chains and the southern Iberian Margin with the External Betic Zone during the middle Miocene. (B) An attempt to compare the tectono-sedimentary evolution of external margins (foredeep stage) in four sectors: (1) External Betic Zone: Proto-Guadalquivir Basin; (2) External Rifian Zone: Proto-Gharb Basin; (3) External Tunisian Tell: post-Numidian foredeep; and (4) Northern Apennines: Marnoso-arenacea Basin.

references therein); and (2) a regional comparison/correlation of the tectono-sedimentary Miocene evolution across the central-western Mediterranean area by means of synthetic and representative external successions reconstructed along the Betic, Maghrebian, and northern Apennine Chains (Figure 10(B)).

The comparison between the study area and other External Betic Zone sectors (Guerrera et al., 2014; Guerrera & Martín-Martín, 2014b; Sissingh, 2008; Vera, 2000) highlights a similar tectono-sedimentary

evolution (Figure 10(B1)). Calcareous and marly formations representing the transition from an internal-external platform realm to a basinal environment are widespread. In deep realms, deposits characterized by olistostromes (Vera, 2000) occur. Several major unconformities linked to the tectonic deformation characterize the middle Burdigalian, Serravallian-Tortonian boundary, and late Tortonian, and related depositional sequences were recognized as pointed out by previous authors (i.e. De Ruig, 1992; Montenat, Ott

D'Estevou, & D'autrey, 1996). The progressive EBZ deformation is presumably related to the NW migration of the Alboran Block (Sanz De Galdeano & Vera, 1992), which is responsible also for the formation of a foredeep depression (proto-Guadalquivir Basin) located between the EBZ and the Iberian Meseta (Figure 10(A)). As shown in Figure 10(B1) the sedimentation in the study area seems to be less continuous regarding that proposed by Vera (2000).

The foredeep evolution in the EBZ (Proto-Guadalquivir foredeep stage) is comparable with the evolution of other external sectors of the Rif (Figure 10(B2)), Tunisian Tell (Figure 10(B3)), and northern Apennine (Figure 10(B4)) Chains (Belayouni et al., 2013; Guerrera, Tramontana, & Donatelli, 2012; Sissingh, 2008; Vera, 2000) that are related to the evolution of several micro-blocks (Alboran, Kabylides, Peloritani and Calabria) resulting from the fragmentation of the Mesomediterranean Microplate (Guerrera & Martín-Martín, 2014a; and references therein), whose Miocene orogenic evolution is schematized in Figure 10(A).

The African Margin shows a younger (late Langhian-Serravallian to Messinian) evolution when compared with the Betic Chain (Figure 10(B3/4)). The Rif sector seems to show two transgressive-regressive cycles (Sissingh, 2008). The lower cycle (late Langhian to middle Tortonian) is represented by the Numidian, Lower Molasse, and Continental Clay Formations, while the upper cycle (late Tortonian-Messinian) consists of the Upper Molasse and Marine Marls Formations, deposited before the emersion. The Tell sector (Belayouni et al., 2013; Salaj & Van Houten, 1988) shows a late Burdigalian-Messinian regressive deposition (Figure 10(B3)) characterized by deep basin (Numidian, Glauconite, and Aingrab-Messiouta Formations), shallow marine (Mahmoud-Hakima and Beglia Formations) and continental (Saouaf lignites Formation) deposits.

The northern Apennine sector (Figure 10(B4)), which shows the youngest evolution (late Langhian-Messinian) and also a regressive trend (Guerrera et al., 2012), is characterized by a deep basin-slope sedimentation (Bisciaro, Schlier, and Marnoso-arenacea Formations).

Another common feature in the compared margins is the occurrence of olithostrome-like or 'salt glacier' deposits related to the overflow of Triassic terrains at different stratigraphic levels coming from the basal level of the stacked superficial nappes or from diapirs, being the latter the most common features placed in the late Miocene (Martín-Martín et al., 2018a, 2018b; Sissingh, 2008; Tent-Manclús et al., 2000).

6. Conclusions

The studied Miocene successions have been better defined with greater resolution.

(1) The Congost Formation (upper Burdigalian p.p.-upper Langhian p.p.) deposited in a marine platform to upper bathyal slope realm while the Lower and Upper Tap Formations (upper Langhian p.p.-middle Tortonian p.p.) was in a deep (basin, and slope) to shallow marine (internal and external platform) realms. Sedimentary and mineralogical data indicate during the early Langhian a marine-vadose environment evolving to an external platform realm. In late Langhian a transition from platform to basin environment occurred. During the Serravallian a sea-level rise generated pelagic environments (SC sector) and in the middle Tortonian a new sea-level fall took place. The comparison of the (S + K):I ratio (synthetic local sea-level curve) with the global sea-level curve reveals minor dissimilarities during the Langhian and a great divergence during the Serravallian, probably induced by the local tectonic activity and predating the Tortonian nappe emplacement.

(2) Two depositional transgressive-regressive sequences (upper Burdigalian p.p.-upper Serravallian p.p. and middle Tortonian p.p. respectively) have been recognized, the lower indicating the transgressive transition from platform to slope realms and the upper showing a regressive trend with development of different platform realms.

(3) The terrigenous supply of the Congost, Lower Tap, and Upper Tap Formations points out a short transport of detrital components from the erosion of uplifting southern internal areas located near the basin. The same clay-mineral association S + I±(I-S) + K found in all the studied SC, PC, and SP successions identifies a same and main source area from the Subbetic Cretaceous-Paleogene terrains, and a continuous minor supply of reworked Triassic materials.

(4) A paleotectonic model and an early Miocene paleogeographic sketch have been proposed (Figure 9). A folding related to a blind thrusting developing during the Burdigalian p.p.-Langhian p.p. is considered contemporaneous to the sedimentation transition from internal to external platform realm. A great variety of platform and slope realms induced by different subsidence rates of the basin together with the growing of anticlines and synclines occurred during the Langhian p.p.-Serravallian. After the early Tortonian regression, platform realms developed in the middle Tortonian. In the same time the emplacement in the southern basinal area of olisthostrome-like deposits is related to emerging thrust systems or rising of diapirs before the complete emplacement of the Subbetic Pila-Nappe.

(5) The Miocene tectono-sedimentary evolution of the External Betic Zone is similar to that recognized in the external sectors of other central-western Mediterranean Chains (Rif, Tell, and northern Apennines). The similarities probably derived from the comparable evolution of different migrating minor blocks (e.g. Alboran, Kabilides, Peloritani and Calabria) originated from the fragmentation of a single microplate (the 'Mesomediterranean

Microplate' *sensu* Guerrera & Martín-Martín, 2014a; *and references therein*) originally located since the late Jurassic between Europe and Africa Plates (Figure 10(A)). The southern margins of this microplate and the northern ones of the African Plate constituted their external domains. In this evolutionary framework a progressive Miocene deformation migrating toward the External Zones of each single system is well recognizable, even if the age of the deformation turns out to be older in the Betic Cordillera and North Africa compared to the Apennines.

(6) The comparison of these evolutionary margins reflects their tectonic complexity which controlled each depositional history together with the relative sea-level changes causing numerous unconformities and gaps.

(7) The tectono-sedimentary evolution of four representative external zones along the Betic, Maghrebian, and Apennine Chains has been included to compare the sedimentary evolutive records and the progressive deformation (Figure 10(B)).

Acknowledgments

Disclosure statement

No potential conflict of interest was reported by the authors.

Funding

ORCID

Manuel Martín-Martín http://orcid.org/0000-0002-5797-9892
Francisco Serrano http://orcid.org/0000-0003-4750-5973
Francisco J. Alcalá http://orcid.org/0000-0002-8165-8669
Mario Tramontana http://orcid.org/0000-0002-7875-6815

References

Alcalá, F. J., Guerrera, F., Martín-Martín, M., Raffaelli, G., & Serrano, F. (2013b). Geodynamic implications derived from numidian-like distal turbidites deposited along the internal-external domain boundary of the Betic Cordillera (S, Spain). *Terra Nova*, 25, 119–129.

Alcalá, F. J., López-Galindo, A., & Martín-Martín, M. (2013a). Clay mineralogy as a tool for sequence-stratigraphy division and detailed paleogeographic reconstructions: An example from upper oligocene-early aquitanian Western Internal South Iberian Margin. *Geological Journal*, 48, 363–375.

Alcalá, F. J., Martín-Martín, M., & López-Galindo, A. (2001). Clay mineralogy of the tertiary sediments in the internal subbetic of Málaga Province (S Spain): Implication for geodynamic evolution. *Clay Minerals*, 36, 615–620.

Arias, C., Castro, J. M., Chacón, B., Company, M., Crespo-Blanc, A., De Federico, D., ... Vilas, L. (2004). Zonas Externas Béticas. In J. A. Vera (ed.), *Geología de España. Sociedad Geológica de España* (pp. 884). España: Instituto Geológico y Minero de España (IGME).

Bally, A. W., & Snelson, S. (1980). Realms and subsidence. In A. D. Miall (Ed.), *Facts and principles of world petroleum occurrence, canadian society of petroleum geologists memoir 6 calgary* (pp. 9–94).

Belayouni, H., Di Staso, A., Guerrera, F., Martin-Martin, M., Miclăus, C., Serrano, F., & Tramontana, M. (2009). Stratigraphic and geochemical study of the organic-rich black shales in the tarcău nappe of the moldavidian domain (Carpathian Chain, Romania). *International Journal of Earth Sciences*, 98, 157–176.

Belayouni, H., Di Staso, A., Guerrera, F., Martin-Martin, M., Serrano, F., & Tramontana, M. (2006). New data about the piedimonte formation (Monte Soro Unit): Insights and constraints to the geodynamic evolution of the sicilian maghrebids. *Geodinamica Acta*, 19/2, 117–133.

Belayouni, H., Guerrera, F., Martín-Martín, M., & Serrano, F. (2013). Paleogeographic and geodynamic Miocene evolution of the Tunisian Tell (Numidian and post-numidian successions): Bearing with the Maghrebian Chain. *International Journal of Earth Sciences*, 102, 831–855.

Blow, W. H. (1969). Late middle Eocene to Recent planktonic foraminiferal biostratigraphy. In P. Bronniman & H. H. Renz (eds.), *Proceedings of the 1st International Conference on Planktonic Microfossils*, Geneva, (Vol. 1, pp. 199–422). Geneva, Swiss. 1967.

Bonardi, G., De Capoa, P., Di Staso, A., Estévez, A., Martín-Martín, M., Martín-Rojas, I., ... Tent-Manclús, J. E. (2003). Oligocene to-early miocene depositional and structural evolution of the calabria–peloritani arc southern terrane (Italy) and geodynamic correlations with the Spain Betics and Morocco Rif. *Geodinamica Acta*, 16, 149–161.

Bosellini, A., Mutti, E., & Ricci-Lucchi, F. (1989). *Rocce e successioni sedimentarie* (XVI, pp. 395). Torino: UTET.

Clark, P. U., Dyke, A. S., Shakun, J. D., Carlson, A. E., Clark, J., Wohlfarth, B., ... McCabe, A. M. (2009). The last glacial maximum. *Science*, 325, 710–714.

Daoudi, L., Deconinck, J. F., Witan, O., & Rey, J. (1995). Impact des variation du niveau marin sur les argiles: Exemple du Crétacé inférieur du bassin d'Essaouira (Maroc). *Comptes Rendus Académie Des Sciences Paris, Série IIa, 320*, 707–711.

De Capoa, P., Di Staso, A., Guerrera, F., Perrone, V., & Tramontana, M. (2003). The extension of the Maghrebian Flysch Basin in the Apenninic Chain: Paleogeographic and paleotectonic implications. *Travaux Institut Des Sciences De Rabat, Géographie Physique*, 21, 77–92.

De Galdeano, S. C., & Vera, J. A. (1992). Stratigraphic record and paleogeographical context of the Neogene basins in the Betic Cordillera, Spain. *Basin Research*, 4, 21–36.

De Ruig, M. J. (1992). *Tectono-sedimentary evolution of the prebetic fold belt of alicante (SE Spain)* (pp. 207). Thesis Vrije University Amsterdam, Amsterdam, Netherlands.

Di Staso, A., Perrotta, S., Guerrera, F., Perrone, V., & Tramontana, M. (2009). New biostratigraphic and petrographic data from the poggio carnaio sandstone Fm (Val Marecchia Nappe): Insights into the tectonic evolution of the Northern Apennines. *Italian Journal of Geosciences*, 128, 443–454.

Di Stefano, A., Foresi, L. M., Lirer, F., Iaccarino, S. M., Turco, E., Amore, F. O., ... Abdul Aziz, H. (2008). Calcareous

plankton high resolution bio-magnetostratigraphy for the Langhian of the Mediterranean area. *Rivista Italiana Di Paleontologia E Stratigrafia*, 114, 51–76.

Dorronsoro, C. (1978). Mineralogical study of the Subbetic Triassic. *Estudios Geológicos*, 34, 251–261.

Garcés, M., Krijgsman, W., & Agustí, J. (2001). Chronostratigraphic framework and evolution of the Fortuna basin (Eastern Betics) since the Late Miocene. *Basin Research*, 13, 199–216.

Guerrera, F., Estévez, A., López-Arcos, M., Martín-Martín, M., Martín-Pérez, J. A., & Serrano, F. (2006). Paleogene tectono-sedimentary evolution of the Alicante Trough (External Betic Zone, SE Spain) and its bearing on the timing of the deformation of the South-Iberian Margin. *Geodinamica Acta*, 19, 87–101.

Guerrera, F., Mancheño, M. A., Martín-Martín, M., Raffaelli, G., Rodríguez-Estrella, T., & Serrano, F. (2014). Paleogene evolution of the external betic zone and geodynamic implications. *Geologica Acta*, 12, 171–192.

Guerrera, F., & Martín-Martín, M. (2014a). Geodynamic events reconstructed in the Betic, maghrebian and apennine chains (central-western Tethys). *Bulletin De La Société Géologique De France*, 185, 329–341.

Guerrera, F., & Martín-Martín, M. (2014b). Paleogene-Aquitanian tectonic breakup in the eastern External Betic Zone (Alicante, SE Spain). *Revista De La Sociedad Geológica De España*, 27, 271–285.

Guerrera, F., Tramontana, M., & Donatelli, U. (2012). Space/time tectono-sedimentary evolution of the umbria-romagna-marche miocene Basin (North Apennines, Italy): A foredeep model. *Swiss Journal of Geosciences*, 105, 325–341.

Haq, B. U., Hardenbol, J., & Vail, P. R. (1987). Chronology of fluctuating sea levels since the Triassic. *Science*, 235, 1156–1167.

Hilgen, F. J., Abels, H. A., Iaccarino, S., Krijgsman, W., Raffi, I., Sprovieri, R., ... Zachariasse, W. J. (2009). The global stratotype section and point (GSSP) of the Serravallian Stage (Middle Miocene). *Episodes*, 32, 152–166.

Hilgen, F. J., Bice, J. S., Iaccarino, S., Krijgsman, W., Montanari, A., & Zachariasse, W. J. (2005). The global stratotype section and point (GSSP) of the tortonian stage (Upper Miocene) at Monte dei Corvi. *Episodes*, 28, 6–17.

Jamoussi, F., Bédir, M., Boukadi, N., Kharbachi, S., Zargouni, F., López-Galindo, A., & Paquet, H. (2003). Répartition des minéraux argileux et contrôle tectono-eustatique dans les bassins de la marge tunisienne. *Compte Rendue De l'Académie Des Science De Paris*, 335, 175–183.

Lancis, C., Tent-Manclus, J. E., Soria, J. M., CaracueL, J. E., Corbí, H., Dinarés-Turell, J., ... Yébenes, A. (2010). Nannoplankton biostratigraphic calibration of the evaporitic events in the Neogene Fortuna Basin (SE Spain). *Geobios*, 43, 201–217.

Lanson, B., Sakharov, B. A., Claret, F., & Drits, V. A. (2009). Diagenetic smectite-to-illite transition in clay-rich sediments: A reappraisal of X-ray diffraction results using the multi-specimen method. *American Journal of Science*, 309, 476–516.

Lourens, L. J., Hilgen, F. J., Laskar, J., Shackleton, N. J., & Wilson, D. (2004). The Neogene Period. In F. M. Gradstein, J. G. Ogg, & A. G. Smith (eds.), *A geologic time scale 2004* (pp. 409–440). Cambridge: Cambridge University Press.

Maaté, S., Alcalá, F. J., Guerrera, F., Hlila, R., Maaté, A., Martín-Martín, M., ... Tramontana, M. (2017). The external tanger unit (Intrarif sub-domain, external rifian zones, Morocco): An interdisciplinary study. *Arabian Journal of Geosciences*, 10, 556.

Martín-Martín, M., Estévez, A., Martín-Rojas, I., Guerrera, F., Alcalá, F. J., Serrano, F., & Tramontana, M. (2018a). The Agost Basin (Betic Cordillera, Alicante province, Spain): A pull-apart basin involving salt tectonics. *International Journal of Earth Sciences*, 107(2), 655–671.

Martín-Martín, M., Guerrera, F., Alcalá, F. J., Serrano, F., & Tramontana, M. (2018b). Source areas evolution in the Neogene Agost Basin (Betic Cordillera): Implications for regional reconstructions. *Italian Journal of Geosciences*, 137. doi:10.3301/IJG.2018.14

Martín-Martín, M., Rey, J., Alcalá, F. J., Tosquella, J., Deramond, J., Lara-Corona, E., ... Antoine, P. O. (2001). Tectonic controls on the deposits of a foreland basin: An example from the Eocene Corbières-Minervois basin, France. *Basin Research*, 13, 419–433.

Montenat, C., Ott D'Estevou, P., & D'autrey, P. (1996). Miocene basins of the eastern Prebetic Zone: Some tectono-sedimentary aspects. In P. F. Friend & C. J. Dabrio (eds.), *Tertiary Basins of Spain. The stratigraphic record of crustal kinematics* (pp. 346–352). Cambridge: Cambridge Univ. Press.

Nadeau, P. H., & Bain, D. C. (1986). Composition of some smectites and diagenetic illitic clays and implications for their origin. *Clays and Clay Minerals*, 34, 455–464.

Perrone, V., Di Staso, A., & Perrotta, S. (2008). The evolution of the western Adriatic margin and contiguous oceanic area: Open problems and working hypotheses. *Bollettino Della Società Geologica Italiana*, 127, 357–373.

Perrone, V., Perrotta, S., Marsaglia, K., Di Staso, A., & Tiberi, V. (2014). The Oligocene ophiolite-derived breccias and sandstones of the Val Marecchia nappe: Insights for paleogeography and evolution of northern Apennines (Italy). *Palaeogeography, Palaeoclimatology, Palaeoecology*, 394, 128–143.

Ruffell, A. H., Price, G. D., Mutterlose, J., Kessels, K., Baraboshkin, E., & Gröcke, D. R. (2002). Palaeoclimate indicators (clay minerals, calcareous nannofossils, stable isotopes) compared from two successions in the late jurassic of the Volga Basin (SE Russia). *Geological Journal*, 37, 17–33.

Salaj, J., & Van Houten, F. B. (1988). Cenozoic palaeogeographic development of Northern Tunisia, with special reference to the stratigraphic record in the Miocene Trough. *Palaeogeography, Palaeoclimatology, Palaeoecology*, 64, 43–57.

Sanz de Galdeano, C., & Buforn, E. (2005). From strike-slip to reverse reactivation: The crevillente fault system and seismicity in the Bullas-Mula area (Betic Cordillera, SE Spain). *Geologica Acta*, 3, 241–250.

Serrano, F., Palmqvist, P., Guerra-Merchán, A., & Romero, A. (1995). Análisis multivariante de las asociaciones de foraminíferos planctónicos de los sedimentos tortonienses de la cuenca de la Atalaya (Cordillera Bética, España). Revista Española de Paleontología. *Sociedad Española de Paleontología (Madrid)*. (Nº Extraord. Homenaje al Dr. Colom) (pp. 119–128).

Sissingh, W. (2008). Punctuated Neogene tectonics and stratigraphy of the African-Iberian plate-boundary zone: Concurrent development of Betic-Rif basins (southern Spain, northern Morocco). *Netherlands Journal of Geosciences*, 87, 241–289.

Tent-Manclús, J. E. (2003). *Estructura y Estratigrafía de las Sierras de Crevillente* (pp. 970). Abanilla y Algayat: su relación con la Falla de Crevillente. Tesis Universidad de Alicante.

Tent-Manclús, J. E., Estévez, A., & Martín-Martín, M. (2000). Olistrostromas originados por laciares de sal al Sur de la Sierra del Cajar (Cuenca neógena de Mula, Murcia). *Geotemas*, 1, 273–276.

Vera, J. A. (2000). El Terciario de la Cordillera Bética: Estado actual de conocimientos. *Revista De La Sociedad Geológica De España*, 12, 345–373.

Vera, J. A. (2004). *Geología de España* (pp. 884). Madrid: IGME-Sociedad Geológica de España Ed.